Cosmological tests of quintessence in quantum gravity

Sukannya Bhattacharya [iD],[a] **Giulia Borghetto**,[b] **Ameek Malhotra** [iD],[b]
Susha Parameswaran [iD],[c] **Gianmassimo Tasinato**[b,d] **and Ivonne Zavala** [iD][b]

[a]*Instituto de Física Téorica UAM/CSIC,*
Calle Nicolás Cabrera 13-15, Cantoblanco, 28049, Madrid, Spain

[b]*Physics Department, Swansea University,*
Swansea, SA2 8PP, U.K.

[c]*Department of Mathematical Sciences, University of Liverpool,*
Liverpool, L69 7ZL, U.K.

[d]*Dipartimento di Fisica e Astronomia, Università di Bologna*
and INFN, Sezione di Bologna,
I.S. FLAG, viale B. Pichat 6/2, 40127 Bologna, Italy

E-mail: sukannya.bhattacharya@ift.csic.es, giulia.borghetto@gmail.com,
ameek.malhotra@swansea.ac.uk, susha.parameswaran@liverpool.ac.uk,
g.tasinato2208@gmail.com, e.i.zavalacarrasco@swansea.ac.uk

ABSTRACT: We use a suite of the most recent cosmological observations to test models of dynamical dark energy motivated by quantum gravity. Specifically, we focus on hilltop quintessence scenarios, able to satisfy theoretical constraints from quantum gravity. We discuss their realisation based on axions, their supersymmetric partners, and Higgs-like string constructions, including dynamical mechanisms to set up initial conditions at the hilltops. We also examine a specific parameterisation for dynamical dark energy suitable for hilltop quintessence. We then perform an analysis based on Markov Chain Monte-Carlo to assess their predictions against CMB, galaxy surveys, and supernova data. We show to what extent current data can distinguish amongst different hilltop set-ups, providing model parameter constraints that are complementary to and synergetic with theoretical bounds from quantum gravity conjectures, as well as model comparisons across the main dark energy candidates in the literature. However, all these constraints are sensitive to priors based on theoretical assumptions about viable regions of parameter space. Consequently, we discuss theoretical challenges in refining these priors, with the aim of maximizing the informative power of current and forthcoming cosmological datasets for testing dark energy scenarios in quantum gravity.

Contents

1 Introduction

One of the most significant and challenging problems in contemporary fundamental physics is to understand the microscopic nature of the Dark Energy (DE) that dominates our Universe today, driving its current accelerated expansion. From one perspective, DE may appear a low-energy problem, since the observed DE scale is small, lying around the milli-eV. However, the fact that vacuum energy — an ultraviolet sensitive quantum phenomenon — behaves

as DE once included in Einstein's General Relativity, frames the problem as a high-energy one. This makes it all the more exciting that cosmological observations are probing the behaviour of DE with an ever-increasing degree of precision, possibly opening a path to connect quantum gravity to observations. In this paper, we consider classes of quintessence models for DE that are currently allowed by quantum gravity considerations, and we test them against the most recent cosmological data. At the same time, we identify trends that current cosmological results indicate for DE model building in quantum gravity.

String theory provides an excellent framework for the DE problem (for reviews, see e.g. [1, 2]). The simplest candidate for DE has long been considered to be a positive vacuum energy (corresponding to a de Sitter vacuum), which, however, must be fine-tuned to a level of one part in 10^{120} — the so-called cosmological constant problem. The supposed String Landscape of exponentially large numbers of finely-spaced metastable de Sitter vacua, together with eternal inflation to populate them, lended itself to an anthropic explanation of this fine-tuning (see e.g. [3] for a review). However, despite impressive technical progress, after two decades of effort there is still no consensus on a single example of an explicit, well-controlled de Sitter vacuum in string theory. Instead, a number of obstructions are invariably met in the hunt for metastable de Sitter string vacua, including challenges in satisfying global and local constraints, tachyonic instabilities, and a lack of parametric or even numerical control in the perturbative expansions used.

At the same time, there has been a growing focus on the expectation that, in string theory and quantum gravity, not everything goes: not every effective field theory (EFT) can be ultraviolet completed into a theory of quantum gravity and those EFTs that are not consistent with quantum gravity are deemed to be in the Swampland. In mapping out which EFTs lie in the Swampland, and which are safely in the Landscape, a number of Swampland Conjectures have been put forward (for recent reviews see e.g. [4–6]). Among them, the de Sitter Swampland Conjecture proposes that (meta)stable de Sitter vacua are inconsistent with quantum gravity. In terms of a string compactification's low energy EFT ingredients, it is supposed that the scalar potential of the string moduli (describing sizes, shapes and positions in the extra dimensions, and the string coupling) should satisfy [7, 8]:

$$\frac{\sqrt{\nabla^a V \nabla_a V}}{V} \geq \frac{c}{M_{\rm Pl}} \qquad \text{or} \qquad \frac{\min(\nabla^a \nabla_b V)}{V} \leq -\frac{c'}{M_{\rm Pl}^2}\,, \qquad (1.1)$$

where "min()" denotes the minimal eigenvalue and c and c' $\mathcal{O}(1)$ positive constants. Whilst there exist physical arguments for these inequalities to hold in asymptotic regions of the moduli space [8] — where large moduli correspond to weak couplings in the corresponding perturbative expansions — the conjecture speculates that it holds everywhere in moduli space. This is not uncontroversial, but it is based on the empirical evidence previously discussed, together with conceptual issues with observers in de Sitter space, such as how to define an S-matrix in this context [9–11].

Conjecture (1.1) rules out a metastable de Sitter vacuum as the explanation for DE, as we cannot have simultaneously $\nabla_a V = 0$, $V > 0$, and eigenvalues$(\nabla^a \nabla_b V) > 0$. The main alternative model for DE is slow-roll quintessence, and a priori it would be natural to expect that quintessence candidates are found amongst the string moduli. Although the conjecture is in tension with the simplest realisations of slow-roll inflation for the early Universe — the

left-hand-sides of (1.1) corresponding directly to the potential slow-roll parameters, ϵ_V and η_V, which need to be small in single-field slow-roll inflation (but see e.g. [12] for potential counter-examples) — it leaves some room to play within the context of late-time quintessence, depending on the values of c and c'. Indeed, whereas around 60 e-folds of inflation in the early Universe are required to solve the horizon problem, the late-time accelerated expansion has been occurring for less than one e-fold of expansion, suggesting a viable window in (1.1). It is important to note, however, that quintessence alternatives remain challenging to obtain in string theory, as they must also satisfy several phenomenological constraints, as well as address the cosmological constant problem.

Keeping these caveats in mind, three distinct classes of simple slow-roll quintessence potentials then come to mind: plateaus, runaways, and hilltops. Plateaus, corresponding to both first and second derivatives of the potential being small, are in tension with (1.1); moreover, they are as difficult to obtain from string theory as metastable dS vacua. Runaway potentials are ubiquitous in string theory, and have both parametric control and a suppressed vacuum energy emerging at the asymptotics of field space. However, generally these potentials turn out to be too steep to source a slow-roll[1] accelerated expansion [13, 14], consistently with the expectation from (1.1) that the slow-roll parameters should be large. Moreover, the small window that could be consistent with (1.1) and slow-roll quintessence does not agree with observations. In fact, string compactifications generically lead to asymptotic exponential potentials, $V(\phi) = V_0 e^{-\lambda\phi}$, which satisfy the conjecture with $\lambda \gtrsim \sqrt{2}$. Such potentials can source a transient late-time accelerated expansion that follows epochs of radiation and matter domination, provided that $\lambda \lesssim \sqrt{3}$ [15], but this parameter space turns out to be ruled out by the most recent cosmological data [16–18]. It is worth emphasising that these results demonstrate a powerful synergy between quantum gravity considerations and cosmological observations: by themselves quantum gravity would allow exponential quintessence with $\sqrt{2} \lesssim \lambda \lesssim \sqrt{3}$ and observations would allow exponential quintessence with $\lambda \lesssim 0.537$ [16]; taken together, exponential runaway quintessence is currently disfavoured. It remains to consider the option of hilltop potentials: this is our aim in this work.

We focus on hilltop quintessence scenarios and explore the interplay between quantum gravity constraints and the most recent cosmological datasets. The models we consider can be made consistent with Conjecture (1.1) as well as other swampland conjectures; moreover, they are expected to arise naturally within string theory. Specifically, we consider axion hilltops, hilltops for a saxion within 4D $\mathcal{N} = 1$ supergravity, and a Higgs-like potential that, close to the hilltop, plays the role of a generic quadratic hilltop. In section 2, we present these general models, motivating their initial conditions; in particular we provide a novel dynamical mechanism to set up the initial conditions for the axion hilltops. After also discussing the connections of the models with string theory and particle physics, in section 3 we review how they can be analysed in a unified way using an appropriate parameterisation of the quintessence equation of state, put forward by Dutta and Scherrer [19] (considering also its generalisation for more general thawing quintessence models by Chiba [20]).

---

[1]Any potential can have some amount of accelerated expansion simply by tuning initial conditions such that the scalar starts by rolling up its potential.

After presenting these general models, motivating their initial conditions, and discussing their connections with string theory and particle physics in section 2, in section 3 we review how they can be analysed in a unified way using an appropriate parameterisation of the quintessence equation of state, put forward by Dutta and Scherrer [19] (considering also its generalisation for more general thawing quintessence models by Chiba [20]). We test this general parameterisation against our concrete scenarios and also show that it provides a useful analytical understanding of the degree of fine-tuning of initial conditions necessary to be consistent with observations.

We are then ready, in section 4, to test our string-motivated hilltop models — together with general hilltops using the Dutta-Scherrer parameterisation — against a suite of recent cosmological data, from CMB observations, galaxy surveys, and Type IA supernovae data. We find the best-fit and mean values and bounds for the fundamental parameters in our models and investigate how these observational constraints stand against independent bounds from quantum gravity considerations. Furthermore, we identify which model is preferred by the data, comparing also to the fits of the ΛCDM model, the exponential runaway model, and the $w_0 w_a$CDM model — the latter corresponding to the alternative Chevakkier-Polarski-Linder (CPL) parameterisation [21, 22], assuming that the equation of state parameter evolves linearly with the scale factor. We summarise our results in section 5, where we also discuss the most important model-building challenges to be addressed in order to extract the maximal information on quantum gravity scenarios from current and forthcoming data sets. A number of technical appendices follows.

2   Quintessence in string theory

In this section we introduce the quintessence models whose cosmologies we study. Importantly, these models are consistent with string theory expectations, but have different interpretations within string theory, and thus distinct associated microscopic parameters with specific interplays with particle physics. After motivating and presenting the models we analyze the associated cosmological equations that will be used in the following sections to confront them with data.[2]

2.1   dS minima, plateaus, runaways, maxima and saddles vs the swampland

As discussed in the introduction, the swampland conjectures on the properties of scalar potentials in string theory (1.1) (and the difficulties in constructing controlled metastable dS string vacua that themselves motivated the conjectures) suggest that the current acceleration of the universe cannot be attributed to a small positive cosmological constant. The same swampland constraints (1.1) are also in tension with a slow-roll quintessence characterised by a scalar potential with a plateau. We have also reviewed how the conjecture (1.1) suggests that runaways are typically too steep to source slow-roll accelerated expansion, and the small window that is allowed is ruled out by observations.

---

[2]In the recent paper [23], model-independent cosmological constraint on c are explored, finding larger-than-one values for this quantity. However, the analysis of [23] does not include hilltops, and the parameter c' is not considered individually. Specifically, [23] focuses on the combined quantity $\Gamma = -c'/c^2$ in the range $\Gamma > 1$, which excludes hilltop scenarios (and exponentials, which have $\Gamma = 1$).

The task is to determine quintessence scenarios that address the previous issues. It is interesting to note that dS maxima and saddles generically satisfy the swampland constraints in (1.1) and, moreover, seem to be easier[3] to find in string constructions compared to dS minima, plateaus and slow-roll runaways. In the following, we will use the term dS "hilltops" to refer to both dS maxima and dS saddles. If one considers a modulus close to a dS hilltop, it can remain frozen by Hubble friction during the epochs of radiation and matter domination, acting as a small cosmological constant, until it only recently starts to slowly roll down its potential sourcing dynamical dark energy. This provides a string-motivated, (thawing[4]) dynamical dark energy candidate,[5] towards which — tantalizingly — recent data seem to hint [28–30].[6] Nevertheless, we stress that the scenarios we discuss do not solve deep theoretical issues as the cosmological constant problem, since they do not directly explain the small size of dark energy density and how the Standard Model contributions are suppressed.

2.2 String models of hilltop quintessence

We will consider three classes of string theory hilltop models, with the quintessence field descending from string moduli or matter fields. Within string theory, two types of moduli — both amongst the most generic predictions of the field content of string scenarios — can be identified as hilltop quintessence candidates:[7]

1. **Axion hilltops.** Axions descend from the dimensional reduction of higher dimensional p-forms, giving rise to the so-called string axiverse[8] [37]. Their scalar potential can be generated by non-perturbative effects such as instantons, with the leading contribution taking the form:

$$V(\theta) = V_0 \left(1 - \cos\left(\frac{\theta}{f}\right) \right) , \qquad (2.1)$$

where f is the axion decay constant, or shift-symmetry breaking scale, and V_0 has an exponential suppression in the instanton action, $V_0 \sim M^4 e^{-S_{\text{inst}}}$, with M the scale of the instanton physics. Both $1/f$ and S_{inst} typically go as the saxionic superpartner for the axion, leading to $f S_{\text{inst}} \sim x M_{\text{Pl}}$ with x an order number [34]. Also, we have assumed (some resolution to the cosmological constant problem and) a Minkowski minimum at $\theta_{\min} = 0$, whilst there is a dS maximum at $\theta_{\max} = \pi f$.

Depending on the value of the decay constant, axion dark energy can occur either (i) close to the minimum of the potential at $\theta = 0$, and up to its inflection point at $\theta = \pi f/2$, which requires $f > M_{\text{Pl}}$, or (ii) near the hilltop at $\theta_{\max} = \pi f$, which allows

---

[3]It should, however, be acknowledged that so far all explicit top-down constructions of dS maxima and saddles involve some size moduli that are smaller than the string-length, implying that they might be spoiled by large α' corrections; see e.g. [24–26]. On the other hand, as we will discuss below, one can make rather general arguments for their existence.

[4]Hilltop quintessence is an example of *thawing* quintessence where w_ϕ starts close to -1 and then increases, as opposed to *freezing* quintessence where w_ϕ starts above -1 and decreases towards it.

[5]See [27] for a recent work on interacting dark energy bounds after DESI.

[6]Of course, we have to wait for future more precise data to have a conclusive answer regarding the dynamical behaviour of dark energy.

[7]Generally, more moduli could be rolling over their potential — however we focus on the simplest case of a single dynamical field.

[8]For early work on axions as quintessence in field theory see e.g. [31–36].

for $f \lesssim M_{\rm Pl}$. We are interested in the latter case, since it allows for values of the decay constant that are usually found in string theory constructions.

Indeed, f has been argued to be always $f \lesssim \mathcal{O}(1)M_{\rm Pl}$ by the so-called weak gravity conjecture [38], which for axions implies that there must exist an instanton whose action satisfies:[9]

$$S_{\rm inst} \lesssim \frac{M_{\rm Pl}}{f} \,, \tag{2.2}$$

In the strong version of the WGC this instanton must be the one with smallest action i.e. the leading effect. To keep control of the instanton expansion assumed in (2.1), we require $S_{\rm inst} > 1$ and thus $f < M_{\rm Pl}$. In the case that $S_{\rm inst} \gg 1$, the exponential suppression in V_0 naturally realises the necessary hierarchy between the dark energy potential and the leading-order potential that fixes the volume moduli.

As pseudo-scalars, axions can evade stringent fifth force constraints even if they are extremely light. Furthermore, their approximate shift symmetries restrict their allowed couplings and protect the axion mass and potential energy density, which are otherwise UV sensitive quantities. An important open question is why initial conditions would be fine-tuned close to the hilltop. One possible mechanism[10] to achieve this is if in the early Universe, the leading non-perturbative effects that are active stabilise the axion in a Minkowsi or adS minimum, and at some later time a further non-perturbative effect dynamically comes into play, turning this minimum into a (nearby) dS maximum (see appendix A.2 for a working example).

2. **Saxion hilltops.** Geometric string moduli, corresponding to sizes and shapes of the extra dimensions and positions within them, as well as the dilaton, also arise generically in string compactifications and are often associated with some small expansion parameter in the low-energy effective field theory description assumed. They also have potentials that include dS maxima and saddles; indeed, one can formulate rather general arguments for the existence of such hilltops. Consider, for example, a compactification that stabilises all moduli in a regime of parametric or numerical control to a supersymmetric AdS vacuum, with one modulus lighter than the others. If the leading correction to the potential at asymptotic values of the light modulus is positive, then a dS maximum must exist to the right of the AdS minimum, and thus also under control [42]. The setup becomes a priori more complex if there is more than one light modulus, since then the minimum may not be accompanied by an extremum in all directions. It is therefore interesting to note that the recent explicit constructions [43] of supersymmetric

---

[9]There is a large literature that attempts to obtain super-Planckian decay constants, usually involving multiple axions for which there exists a generalised mutifield weak gravity conjecture (WGC). The axion alignment mechnism [39] invokes two (or more) axions and a fine-tuning between their axion decay constants that produces a large effective axion decay constant. In N-flation [40], a large number N of axions, each with axion decay constant f, lead to an effective axion decay constant $f_{\rm eff} = \sqrt{N}f$. However, both axion alignment and N-flation require some extra model building to satisfy the multifield WGC, and in any case violate the strong WGC. See e.g. [4] for a further discussion of the literature, including top-down model building attempts, where the challenges encountered may well seem consistent with a quantum gravity censorship of large axion decay constants.

[10]See [41] for an alternative dynamical mechanism for the QCD axion.

AdS minima in type IIB flux compactifications with many moduli — which are under numerical control[11] — have been found to be accompanied by dS maxima.

For concreteness, in the following, we consider a specific, simple saxion hilltop model that is well-motivated from supergravity and was studied recently in [44]. This model starts with a supersymmetric Minkowski setup with one flat direction, which is lifted by a leading-order supersymmetry-breaking non-perturbative contribution, with details given in appendix A. The corresponding scalar potential, expressed in terms of the canonical normalised field, is given by:

$$V(\phi) = V_0 \, e^{-\sqrt{2}\phi} \, e^{-2\alpha e^{\sqrt{2}\phi}} \left(-2 + 4\,\alpha^2 e^{2\sqrt{2}\phi} + 4\,\alpha\,e^{\sqrt{2}\phi} \right) , \qquad (2.3)$$

with α a constant that depends on the type of non-perturbative effect in play. For example, for gaugino condensation in a hidden $SU(N)$ gauge group (from wrapped D7-branes) in type IIB string models, we have $\alpha = 2\pi/N$. The scalar potential (2.3) has a maximum at:

$$\phi_{\text{max}} = \frac{1}{\sqrt{2}} \log\left(\frac{1}{\sqrt{2}\alpha} \right) , \qquad (2.4)$$

which lies in a "weak-coupling" regime, say $\phi_{\text{max}} \gtrsim 0.4$ for the canonically normalised field,[12] for around $\alpha \lesssim 0.4$, or $N \gtrsim 16$. Note that geometrical and topological constraints imply that N cannot be arbitrarily large,[13] but we can safely take, say, $N \lesssim \mathcal{O}(100)$. On the other hand, as discussed in appendix A, we can in any case expect at best numerical control of the expansion in the non-perturbative effects at the hilltop.

Although the exponential suppression in the saxion potential energy turns out to cancel at ϕ_{max}, its scale can match the observed dark energy by being multiply exponentially suppressed in the vevs of the supersymmetrically stabilised moduli [24]. Saxions do not enjoy a shift symmetry like the axions, but constraints from time variation of fundamental constants, fifth forces and radiative corrections can potentially be avoided if the quintessence couples only indirectly, via gravity and with some further geometric suppression, to the Standard Model and the supersymmetry breaking sector. The fine-tuning of initial conditions could be explained e.g. via high temperature effects [47] or some other dynamics [48] turning the maximum into a transient minimum analogously to symmetry restoration in the Higgs potential; alternatively, anthropic arguments

---

[11]Note that — even though the solutions in [43] include some two-cycle volumes that are small (cf. footnote 3) — it has been checked explicitly that e.g. the worldsheet instanton expansions are under control. Moreover, whilst control of the dS minima (a.k.a. "KKLT vacua") in [43] is under question because the concrete examples have $g_s M \lesssim 1$, this regime is only of concern in the presence of a warped throat, in which case the supergravity expansion breaks down. The warped throat is a necessary ingredient for the KKLT dS minimum, but not for the precursor supersymmetric AdS vacuum of interest here.

[12]This corresponds to the original field $\varphi_{\text{max}} \gtrsim 1.8$ (see (A.5)).

[13]E.g. for gaugino condensation from wrapped D7-branes in type IIB, [45] (see also [46]) found that $N \lesssim \mathcal{O}(10)h^{1,1}$ with $h^{1,1}$ related to the number of size moduli of the compactification (more explicitly, $h^{1,1}$ is the Hodge number of the Calabi-Yau manifold counting for the number of Kähler moduli).

might be relevant, since without fine-tuning to the hilltop, the saxion would runaway to decompactification or decoupling and an unviable universe.[14]

In what follows, we explore hilltop quintessence using the two concrete moduli examples above — the axion hilltop and the supergravity saxion hilltop — together with a more generic Higgs-like quadratic hilltop, which can approximate any quadratic hilltop near the top, and which might descend from a stringy saxion modulus, stringy axion modulus, or a stringy matter field:

3. **Higgs-like hilltops.** The dynamics from any quadratic hilltop potential can be approximated by using a Higgs-like potential

$$V(\phi) = V_0 \left(1 - \left[\frac{\phi}{\phi_0} \right]^2 \right)^2 . \qquad (2.5)$$

This potential is bounded from below by having a quartic term compared to the more standard quadratic field theory hilltops. This — and any other terms that might appear in the Taylor expansion of the hilltop potential about its maximum — will not affect the dynamics for as long as the field stays sufficiently close to its hilltop.

Should the field ϕ explore a significant part of its field-range, the swampland distance conjecture [50] would limit $\phi_0 \lesssim \mathcal{O}(1) M_{\text{Pl}}$. In hilltop quintessence scenarios, ϕ remains frozen for most of the cosmological history, allowing this constraint to be relaxed.

We focus on the cosmological aspects of the hilltop quintessence models, from the cosmological evolution and comparison with cosmological observations in the CMB, galaxy surveys and type IA supernovae catalogues, to a discussion on the initial conditions and implications for inflation and reheating. We aim to ascertain to what extent theoretical and observational constraints might favour a specific model of hilltop quintessence, and what insights observational constraints give into the microscopic parameters of stringy hilltop quintessence models.

2.3 Cosmological equations for hilltop quintessence

We now set up the equations of motion that describe the background cosmological evolution for the models of interest. We consider a universe whose dark energy (DE) component is described microscopically by one of the hilltop quintessence fields introduced above, with a canonical kinetic term and a scalar potential functional $V(\phi)$, minimally coupled to gravity. We further include radiation and (dark) matter and — though we do not consider the detailed string theory model building required to achieve it — we assume that they are decoupled from the quintessence field. Given theoretical expectations and observational prospects, we also allow for non-zero curvature of the 3D space slices at this stage.[15]

---

[14]These arguments do not work in the same straightforward way for axions. E.g. the axion's remnant discrete shift symmetry implies that axion-matter couplings are such that finite temperatures, and other dynamical effects, typically only change the effective axion-mass and not the position of the minima in axion potentials (see e.g. [47, 49]). Also, relaxing initial conditions away from the hilltop would lead to the axion rolling down to a minimum whose vacuum energy is of similar magnitude to that at the maximum and hence equally anthropically viable.

[15]For completeness, in appendix C we collect the cosmological evolution including curvature.

The 4D FLRW metric with arbitrary curvature given is given by:

$$ds^2 = -dt^2 + a^2(t) \left(\frac{dr^2}{1 - kr^2} + r^2 \left[d\theta^2 + \sin^2\theta d\varphi^2 \right] \right) , \tag{2.6}$$

where $k = 0, \pm 1$ denotes the curvature of the 3D slices. The energy momentum tensor is described by a set of perfect fluids describing the radiation, matter, quintessence, and effective "curvature fluid" components. The energy density and pressure, ρ_i, p_i, for these components are related by their *equation of state parameter*, w_i, as:

$$p_i = w_i \rho_i , \tag{2.7}$$

where $i = r, m, \phi, k$ runs over radiation, matter, quintessence, and curvature; $w_r = \frac{1}{3}$ and $w_m = 0$, whilst for the scalar:

$$\rho_\phi = \frac{\dot{\phi}^2}{2} + V(\phi) , \qquad p_\phi = \frac{\dot{\phi}^2}{2} - V(\phi) , \qquad w_\phi = \frac{p_\phi}{\rho_\phi} , \tag{2.8}$$

and for the curvature component:

$$\rho_k = -\frac{3\,k}{a^2} , \qquad p_k = \frac{k}{a^2} , \qquad w_k = -\frac{1}{3} . \tag{2.9}$$

We can now write down the cosmological equations of motion for this system, which are given by (we set $\kappa = 8\pi G_N = 1$ for now):

$$H^2 = \frac{\rho_{\text{eff}}}{3} , \tag{2.10a}$$

$$\frac{\ddot{a}}{a} = -\frac{\rho_{\text{eff}}}{6}(1 + 3w_{\text{eff}}) , \tag{2.10b}$$

$$\ddot{\phi} = -3H\dot{\phi} - V_\phi . \tag{2.10c}$$

In the last equation, $V_\phi \equiv \partial_\phi V$. Moreover, we defined

$$\rho_{\text{eff}} = \sum_i \rho_i , \qquad p_{\text{eff}} = \sum_i p_i , \qquad p_{\text{eff}} = w_{\text{eff}}\, \rho_{\text{eff}} . \tag{2.11}$$

From this definition it is clear that

$$w_{\text{eff}} = \sum_i w_i \Omega_i , \tag{2.12}$$

where

$$\Omega_i = \frac{\rho_i}{3H^2} . \tag{2.13}$$

Moreover, from (2.10b), we learn that acceleration requires $w_{\text{eff}} < -1/3$.

3   Parameterisation of the equation of state for hilltop models

In all hilltop quintessence models, the quintessence field is initially frozen by Hubble friction close to the hilltop and starts to slowly roll, as the Universe expands and Hubble friction falls, in recent times. All hilltop quintessence potentials are therefore well-approximated

for the full cosmological history by their behaviour close to the hilltop, i.e. their Taylor expansion around the maximum up to second order. It is therefore not surprising that all hilltop models can be described in a universal way. In fact, Dutta and Scherrer have derived in [19] a parameterisation of the equation of state parameter for hilltop quintessence models, and Chiba has shown in [20] that this parameterisation can actually be extended to more general thawing quintessence models.

In this section, we first outline the derivation of the Dutta-Scherrer(-Chiba) (DS(Ch)) parameterisation and then test how it fairs for the specific hilltop models in our focus, showing that it performs much better than the more commonly used CPL parametersation [21, 22]. For comparison, we also test the DSCh parameterisation against a quintessence model without hilltop, specifically with an exponential potential. Finally, we use the DS parameterisation to obtain a bound on the initial displacement from the hilltop, which, as expected, depends on the curvature at the hilltop. As we will show, this subsequently leads to a bound on the scale of inflation or reheating.

3.1 Derivation of the Dutta-Scherrer(-Chiba) (DSCh) parameterisation

Dutta and Scherrer obtained their parameterisation of the equation of state parameter for hilltop quintessence by computing the general solution to the scalar field in a flat universe whose dynamics is dominated by the scalar and matter. We now outline the calculation of DS [19], pointing out along the way how the derivation also applies in the presence of curvature, so long as the curvature is subdominant, as it is in our observed universe. As already mentioned, the beauty of the DS parameterisation is that it is analytically justified for generic hilltop potentials, which can all be approximated by the same Taylor expansion around the maximum as:

$$V(\phi) \approx V(\phi_{\max}) + \frac{1}{2}V''(\phi_{\max})(\phi - \phi_{\max})^2 \,. \tag{3.1}$$

To begin, we consider the scalar field equation, (2.10c), in the background of matter and the hilltop potential energy, which corresponds to an effective cosmological constant $\Lambda = V(\phi_{\max})$. That is, we assume that the rolling of the scalar field away from its hilltop hardly affects the overall background expansion of the Universe, and moreover, that radiation and curvature are negligible during the epochs of interest. Note that the energy density from the curvature grows more slowly than that from radiation and matter as one tracks backwards in time, so if the curvature is subdominant today — as it is — then it was subdominant throughout the history of the universe. Given our assumed background cosmology, which is effectively a flat ΛCDM (i.e. neglecting the subdominant radiation, curvature and time-varying quintessence), the expansion as a function of time is given by:

$$\frac{a(t)}{a_0} = \left[\frac{1 - \Omega_{\Lambda,0}}{\Omega_{\Lambda,0}}\right]^{1/3} \sinh^{2/3}(t/t_\Lambda) \,, \tag{3.2}$$

where a_0 is the scale-factor today, we denoted the present-day density parameter from the hilltop potential energy as $\Omega_{\Lambda,0}$, and defined

$$t_\Lambda \equiv \frac{2}{3H_0\sqrt{\Omega_{\Lambda,0}}} = \frac{2}{\sqrt{3V_{\max}}} \,, \tag{3.3}$$

with $V_{\max} \equiv V(\phi_{\max})$. Let us now define a new variable $u(t)$ as follows [19]:

$$u(t) = (\phi - \phi_{\max})a^{3/2}(t). \tag{3.4}$$

In terms of u, the equation for ϕ (2.10c) becomes

$$\ddot{u} - \frac{3}{2}u\left[\frac{\ddot{a}}{a} + \frac{1}{2}H^2\right] + a^{3/2}V_\phi = 0. \tag{3.5}$$

Using (2.10a) and (2.10b), this becomes

$$\ddot{u} + \frac{3}{4}u\,p_{\text{eff}} + a^{3/2}V_\phi = 0, \tag{3.6}$$

where remember that we are assuming that p_{eff} includes only the contribution from the hilltop maximum (with $w_\Lambda = -1$) and matter (with $w_m = 0$) and therefore:

$$p_{\text{eff}} \simeq -V_{\max}. \tag{3.7}$$

Recalling the expansion (3.1), and writing $V''_{\max} \equiv V''(\phi_{\max})$, we have $V_\phi = V''_{\max}(\phi - \phi_{\max})$. Therefore, (3.6) can be reduced to:

$$\ddot{u} + u\left[V''_{\max} - \frac{3}{4}V_{\max}\right] = 0. \tag{3.8}$$

Defining

$$k_V \equiv \sqrt{\frac{3}{4}V_{\max} - V''_{\max}}\ , \tag{3.9}$$

the general solution to (3.8) is given by

$$u(t) = A\,\sinh(k_V t) + B\cosh(k_V t). \tag{3.10}$$

To fix the integration constants, consider an initial, finite value for ϕ at $t = 0$:

$$\phi(0) \equiv \phi_i \equiv \phi_{\max} + \Delta\phi_i. \tag{3.11}$$

Then (3.4) together with (3.2) requires $B = 0$ in (3.10), and also fixes the value of A in terms of $\Delta\phi_i$, giving the final solution for $\phi = \phi_{\max} + u/a^{3/2}$:

$$\phi = \phi_{\max} + \frac{\Delta\phi_i}{K}\frac{\sinh(k_V t)}{\sinh(t/t_\Lambda)}, \tag{3.12}$$

where we defined

$$K \equiv k_V t_\Lambda. \tag{3.13}$$

The next step is to find an expression for the equation of state parameter associated to ϕ as a function of a, $w_\phi(a)$. First notice that

$$1 + w_\phi = \frac{\dot{\phi}^2}{\rho_\phi} \simeq \frac{\dot{\phi}^2}{V_{\max}}, \tag{3.14}$$

where we used the approximation that $\rho_\phi \simeq V_{\max}$. Normalising this expression to the present-day value of w_ϕ, denoted by w_0, and using the solutions for ϕ and the scale factor a, eqs. (3.12) and (3.2), one arrives at the final expression as in [19]:

$$\frac{1 + w_\phi(a)}{1 + w_0} = \left(\frac{a}{a_0}\right)^{3(K-1)} \left[\frac{(K - F(a))(1 + F(a))^K + (K + F(a))(F(a) - 1)^K}{(K - F_0)(1 + F_0)^K + (K + F_0)(F_0 - 1)^K}\right]^2 , \quad (3.15)$$

where, approximating $\Omega_{\Lambda,0} \simeq \Omega_{\phi,0}$:

$$K = \sqrt{1 - \frac{4}{3}\frac{V''_{\max}}{V_{\max}}}, \quad (3.16a)$$

$$F(a) \equiv \sqrt{1 + \left(\frac{a}{a_0}\right)^{-3}\left(\frac{1 - \Omega_{\phi,0}}{\Omega_{\phi,0}}\right)}, \qquad F_0 = F(a_0). \quad (3.16b)$$

We see that the parameterisation involves two free parameters: K, which depends on the curvature of the potential around the hilltop as in (3.16a); and w_0, which depends on K and the initial displacement of the scalar field from its maximum, $\Delta\phi_i$, as:

$$1 + w_0 = \frac{3}{16}\frac{\Delta\phi_i^2}{K^2}\frac{(1 - \Omega_{\phi,0})}{\Omega_{\phi,0}}\left[(K - F_0)\left(\frac{1 + \sqrt{\Omega_{\phi,0}}}{\sqrt{1 - \Omega_{\phi,0}}}\right)^K + (K + F_0)\left(\frac{1 - \sqrt{\Omega_{\phi,0}}}{\sqrt{1 - \Omega_{\phi,0}}}\right)^K\right]^2 . \quad (3.17)$$

Chiba's generalization of (3.15) [20] purports to extend the validity of the parameterisation beyond hilltops to general thawing quintessence models by allowing the field to start at some arbitrary initial value, ϕ_i, and keeping all terms in the Taylor expansion of the potential around $V(\phi_i)$ up to second order (cf. (3.1)). Formally, this parameterisation ends up coinciding with (3.15), but with K in (3.16a) defined via the initial values of V''_i and V_i, rather than their values at the maximum. On the other hand, it is not obvious why — if both first and second order terms in the Taylor expansion are significant — third order terms and beyond can be neglected.

It is interesting to compare the DSCh parameterisation with the commonly used linear CPL parameterisation [21, 22], with parameters w_0 and w_a:

$$w_\phi(a) = w_0 + (1 - a)w_a , \quad (3.18)$$

which — though it lacks the analytical justification of the DS parameterisation for hilltops — is based on a Taylor expansion of the equation of state parameter itself, where the leading term is the linear one. In the following, we test the DS(Ch) (3.15) and CPL (3.18) parameterisations against both hilltop models and the exponential runaway potential, using the modification by Chiba [20] for the latter. A comparison of different phenomenological parameterisations was performed in [51] for a particular hilltop model with $V(\phi) = V_0\, e^{-c\phi}(1 + \alpha\phi)$, while the DSCh parameterisation was analysed against recent data in [52].

3.2 Testing the DS parameterisation for hilltop quintessence models

In this section, we test the DS [19] parameterisation against the explicit hilltop models presented in section 2. For comparison, in the next subsection 3.3, we test the parameterisation also against the exponential dark energy model, using the Chiba [20] generalisation.

We start by checking how the parameter K in the DS parameterisation is related to the more fundamental parameters in the different models that we are interested in analysing:

1. **Axion hilltops**. The scalar potential is given by (2.1) and for hilltop quintessence, we are interested in the case $f \lesssim 1$, which is also consistent with typical values found in string theory and suggested by swampland constraints [38]. For this model, the parameter K is given by:

$$K_{\rm ax} = \sqrt{1 + \frac{2}{3f^2}} \,. \tag{3.19}$$

Thus for $f \lesssim 1$, $K_{\rm ax} \gtrsim \sqrt{5/3} \sim 1.3$. In figure 1 we compare the true evolution of the equation of state parameter obtained using CAMB with the DS and CPL parameterisations, for the best-fit value of the decay constant using DESI year one data plus Union3 supernova data, $f = 0.15$ (see table 6 in appendix B), and for $f = 0.5$. As we commented before, since the spatial curvature k is subdominant throughout the cosmological evolution, adding a small non-zero k does not change the results. We collect the evolution with non-zero spatial curvature in appendix C.

As we can see from the figure 1, the DS parameterisation works very well through the full cosmological evolution, well beyond the reach of current and near-future Dark Energy surveys; indeed, the derivation of the DSCh parameterisation suggests that it should work as soon as radiation is negligible (and recall that $z_{eq} \approx 3400$). In the figures, the evolution starts in the matter domination epoch from $z_m = 3000$. For the CPL parameterisation we fit the linear behaviour to obtain suitable values of w_0, w_a. It is very clear that the linear parameterisation (3.18) is not appropriate for axion hilltop quintessence throughout the evolution; rather it works only for small red-shifts as f decreases. We will see the same pattern also for the other hilltop potentials below.

Finally, in figure 2, we compare the evolution of the dark energy equation of state for different initial conditions as indicated in the plot.

2. **Saxion hilltop**. The potential of this model is given by (2.3) [44], where typical values for α are $\frac{2\pi}{N}$ with, recall, N an integer that we assume to be $N \lesssim \mathcal{O}(100)$. Interestingly, for this model, K is independent of the potential parameters! Indeed,

$$K_{\rm sugra} = \sqrt{\frac{19 + 8\sqrt{2}}{3}} \simeq 3.179 \,, \tag{3.20}$$

and thus the curvature at the maximum is independent of α and the evolution will mostly be dependent on ϕ_i. To better understand the constraints on α in this case, it is useful to write the potential as follows:

$$V = \frac{e^{-\sqrt{2}}}{3} V_0 \, \alpha \left[a_0 - a_2 \, \kappa^2 \phi_{\rm max}^2 \left(\frac{\phi}{\phi_{\rm max}} - 1 \right)^2 + a_3 \, \kappa^3 \phi_{\rm max}^3 \left(\frac{\phi}{\phi_{\rm max}} - 1 \right)^3 + \dots \right], \tag{3.21}$$

where we restored Planck units $\kappa = 1/M_{\rm Pl}$, a_n are numerical constants independent of α given by $a_0 = 12$, $a_2 = 12(2 + \sqrt{2})$ and $a_3 = 32$, and recall that $\phi_{\rm max}$ is given in terms of α by (2.4). Note that $\phi_{\rm max}$ can be positive or negative, depending on the
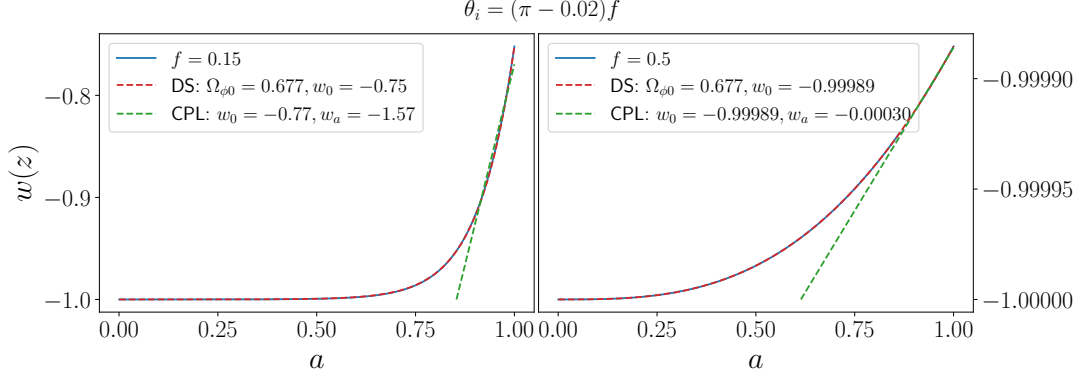
Figure 1. Evolution of the equation of state parameter for the axion hilltop for different values of f, and its comparison to the DS (3.15) and CPL (3.18) parameterisations. The initial value for θ is given at the top of the plots and for the DS parameterisation we used the values of $\Omega_{\phi 0}$ and w_0 as indicated to the right, as obtained from the evolution with CAMB. The CPL parameters are obtained by fitting the linear behaviour between $a = 0.9$ and $a = 1$.
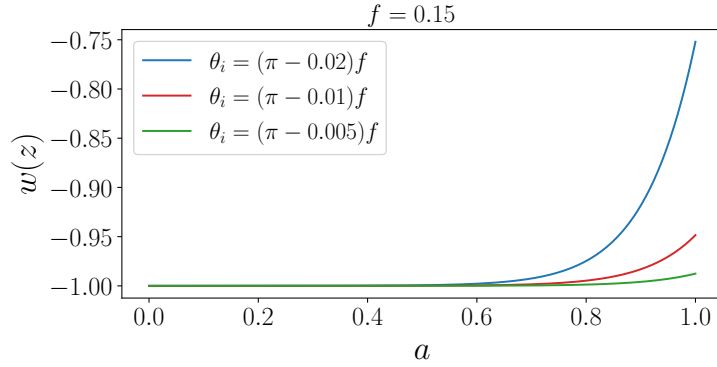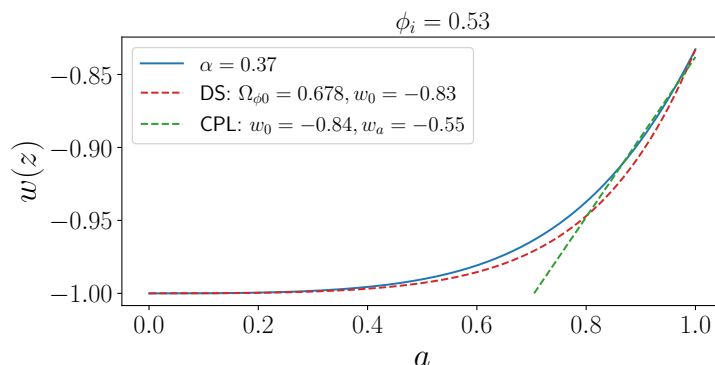

Figure 2. Evolution of the equation of state parameter for the axion hilltop for different initial conditions θ_i.

value of α (see eq. (2.4)). In particular for $\alpha \geq 1/\sqrt{2}$, $\phi_{\max} \leq 0$. On the other hand, $\phi_{\max}$ becomes super-Planckian for $\alpha \lesssim 0.17 \sim \frac{2\pi}{37}$. As we mentioned before, α is also constrained by ensuring theoretical control to $\alpha \lesssim 0.4$. Therefore in the next section we will focus on $\alpha \in \left(\frac{2\pi}{32}, \frac{2\pi}{9} \right)$.

From the expansion around the maximum (3.21), we also see that contrary to the axion and field theory Higgs-like model, there is a non-zero cubic contribution. Thus, for $\phi/\phi_{\max} < 1$, the cubic term changes sign, as the potential becomes steeper (and unbounded) on the left hand side. (On the other hand, the axion and Higgs potentials have the same curvature to either side). Due to the cubic contribution, we expect the DS parameterisation to be a little less accurate in this case, compared to the axion and Higgs.

In figure 3 we compare the evolution of the equation of state with the DS and CPL parameterisations, using the best-fit value for the parameter α obtained from DESI year

Figure 3. Evolution of the equation of state parameter for the supergravity hilltop and its comparison to the DS (3.15) and CPL (3.18) parameterisations. The initial value for the saxion is given at the top of the plot. For the DS parameterisation we used the values of $\Omega_{\phi 0}$, w_0 obtained from the evolution with `CAMB` as indicated to the right, while we fit the linear behaviour between $a = 0.9$ and $a = 1$ to obtain (w_0, w_a).
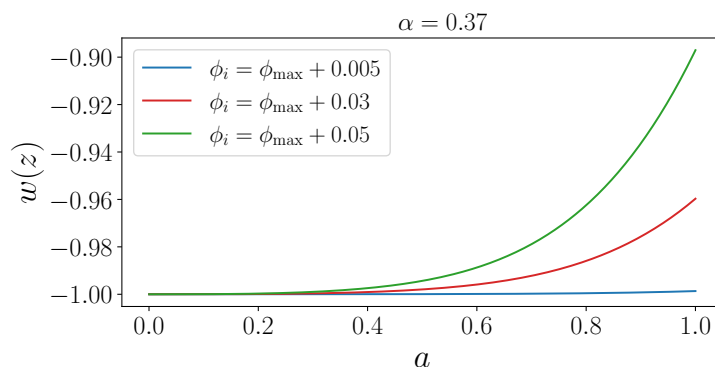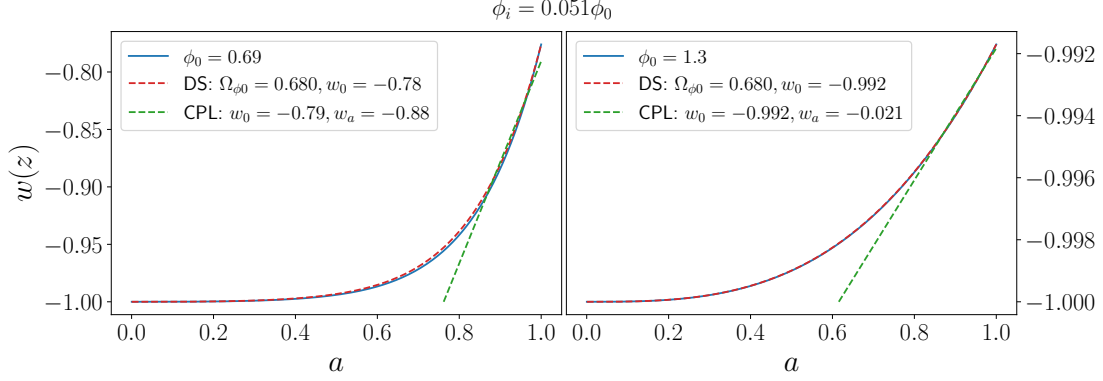

Figure 4. Evolution of the equation of state parameter for the supergravity hilltop for different initial conditions ϕ_i.

one data plus Union3 supernova data i.e. $\alpha = 0.37 \sim \frac{2\pi}{17}$ (see table 7 in appendix B). From the figure we see that the DS parameterisation does slightly worse here compared to the Axion (see figure 1) and Higgs (see figure 5) cases, through the full cosmological evolution, whereas the linear parameterisation breaks down rather quickly.
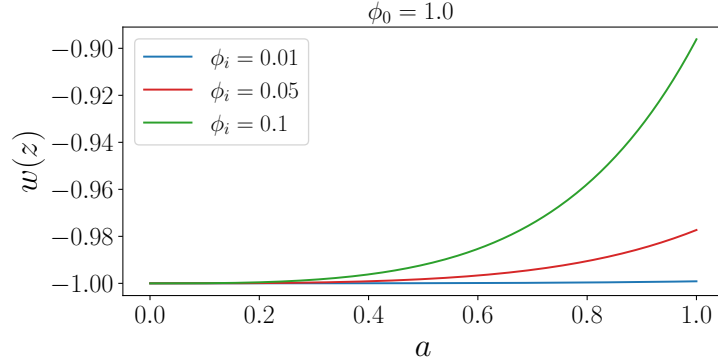
In figure 4, we compare the evolution of the dark energy equation of state for the saxion model, for different initial conditions.

3. **Higgs-like hilltop.** The potential for this model is given by (2.5), where recall that in order to avoid issues with the numerical and cosmological analysis, we completed the quadratic hilltop to a Higgs-like potential. For this potential, K is given by

$$K_{\text{Higgs}} = \sqrt{1 + \frac{16}{3\phi_0^2}}\,. \tag{3.22}$$

– 15 –

Figure 5. Evolution of the equation of state parameter for the Higgs-like hilltop (2.5) and its comparison to the DS (3.15) and (3.18) parameterisations. For DS we used $\Omega_{\phi 0}$, w_0 as obtained from the evolution with `CAMB`, while we fitted the linear behaviour between $a = 0.9$ and $a = 1$ for the CPL to obtain (w_0, w_a) as indicated to the right. The initial value for the scalar field is indicated at the top of the plot.
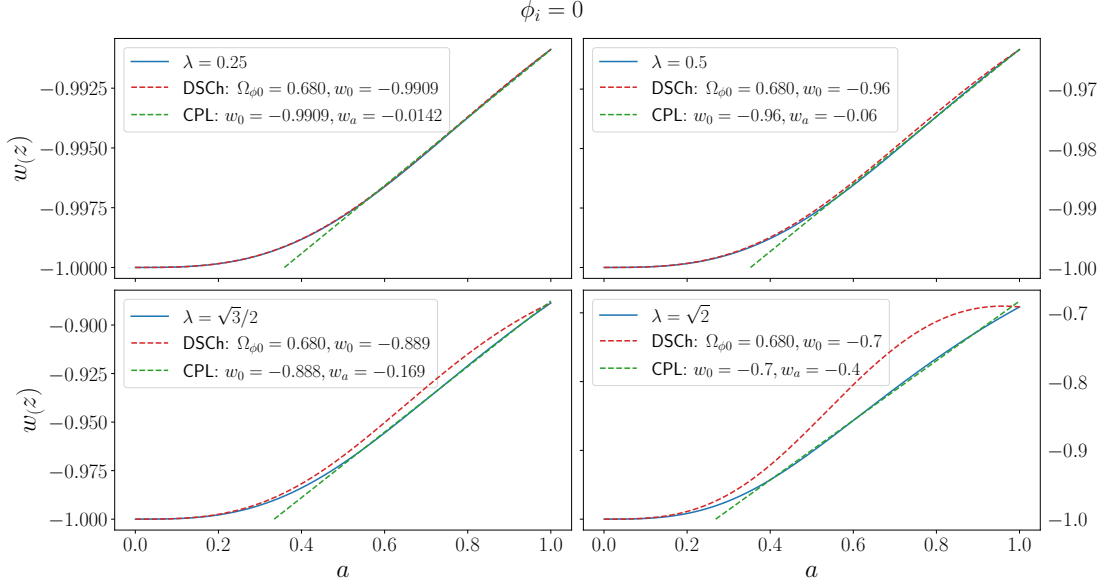

Figure 6. Evolution of the equation of state parameter for the Higgs-like hilltop for different initial conditions, ϕ_i.

If we expect ϕ_0 to be less than or at most one (recall we are using Planck units), $\phi_0 \lesssim 1$, then $K_{\text{Higgs}} \gtrsim \sqrt{19/3} \sim 2.5$.

In figure 5 we compare the evolution of the equation of state with the DS and CPL parameterisations, for the best-fit value of $\phi_0 = 0.69$ using from DESI year one data plus Union3 supernova data (see table 8 in appendix B) and for $\phi_0 = 1.3$. Again, we learn that the DS parameterisation works very well through the full cosmological evolution also in this example, whereas the CLP parameterisation works only for smaller redshifts.

Finally in figure 6 we compare the evolution of the equation of state for the field theory model for different values of ϕ_i.

Figure 7. Evolution of the equation of state parameter for the exponential potential (3.1) and its comparison to the DSCh and CPL parameterisations. For the latter we used $\Omega_{\phi 0}$, w_0 obtained from the evolution with CAMB, while for CPL we fitted the linear behaviour between $a = 0.5$ and $a = 1$ to obtain the parameters, indicated to the right.

3.3 Comparison: testing DSCh parameterisation in exponential quintessence

For comparison, having verified the success of the DS parameterisation for various explicit hilltop models, we now test how its generalisation by Chiba fares with a potential that does not have a maximum. We do this using an exponential potential, whose cosmology has recently been studied in [16, 17, 53]:

$$V = V_0 \, e^{-\lambda\phi} \, . \tag{3.23}$$

Recall that the DSCh parameterisation corresponds to (3.15) where $V_{\max}, V''_{\max}$ in K are replaced by $V_i = V(\phi_i), V''_i = V''(\phi_i)$. Though in general K will depend on ϕ_i, for the exponential case, it is independent of it, becoming purely dependent on λ:

$$K_{\exp} = \sqrt{1 - \frac{4\lambda^2}{3}} \, . \tag{3.24}$$

Note that $K_{\exp}^2$ can be negative, giving rise to oscillatory behaviour in the parameterisation [20]. In this case, one should replace $K \to i\tilde{K}$ with $\tilde{K} = \sqrt{4V''_i/3V_i - 1}$ in (3.15). Interestingly, $K_{\exp}^2 < 0$ for $\lambda > \sqrt{3}/2 \sim 0.866$. In figure 7 we compare the evolution of the equation of state with the DSCh and CPL parameterisations for different values of λ. As we can see from the comparison, the DS parameterisation works rather well for $K_{\exp}^2 > 0$, but it does not do well for $K_{\exp}^2 < 0$. For $K_{\exp}^2 > 0$, the DSCh parameterisation works out to larger redshifts than the linear CPL parameterisation, but for $K_{\exp}^2 < 0$ the CPL parameterisation does better.

3.4 Bounds on — and from — the initial conditions

As we have anticipated, a problem particular to hilltop quintessence is the fine-tuning of initial conditions close to the dS maximum. Intuitively, the higher the curvature of the hilltop, the closer to the hilltop ϕ needs to start in order to drive cosmic acceleration. Even if such initial conditions can be selected via some physical mechanism in the early universe before big bang nucleosynthesis — e.g. dynamically or anthropically — they need to subsequently survive quantum diffusion effects. The DS parameterisation provides us with an analytical expression for the initial displacement from the top of the potential, $\Delta\phi_i$, in terms of the curvature of the potential at the hilltop, K, the equation of state parameter today, w_0, and the density parameter for quintessence today, $\Omega_{\phi,0}$:

$$\Delta\phi_i = 4K\Omega_{\phi,0}\sqrt{\frac{(1+w_0)}{3}}\frac{(1-\Omega_{\phi,0})^{\frac{K-1}{2}}}{\left(K\sqrt{\Omega_{\phi,0}}-1\right)\left(1+\sqrt{\Omega_{\phi,0}}\right)^K+\left(K\sqrt{\Omega_{\phi,0}}+1\right)\left(1-\sqrt{\Omega_{\phi,0}}\right)^K}\,.$$

(3.25)

Note that as w_0 increases from -1 to 1, $\Delta\phi_i$ also grows, and as $\Omega_{\phi,0}$ increases from 0 to 1, $\Delta\phi_i$ decreases. Although the overall dependence on K is complex, it is clear that the larger the value of K (function of the hilltop curvature in (3.16a)), the larger the curvature, and therefore, the smaller initial displacement from the hilltop (smaller $|\Delta\phi_i|$) is expected. We make manifest such behaviour with figure 8, where we plot the K-dependence of $|\Delta\phi_i|$ using the best-fit values for w_0 and Ω_{ϕ_0} (see table 9) from the cosmological analysis described in subsection 4.4, together with the derived 1σ and 2σ limits on the derived parameter $|\Delta\phi_i|$. In the same plot we include the predictions for different hilltop quintessence models.

The 2σ tail extending towards larger $|\Delta\phi_i|$ in figure 8 is expected, since very small curvature is still allowed when ϕ_i is far away from the hilltop, and, in fact, this tail follows the analytical curve. This asymmetric part in 2σ eventually leads to the skewed posterior distribution for small K values shown in figure 12 in next section.

Once the best-fit value of the displacement from the hilltop inferred from the cosmological data has been found, this in turn sets an upper bound on the Hubble scale at the end of reheating, if we assume that the initial conditions were set up by this time. Indeed, for quantum diffusion at around the time of reheating — and thus any time thereafter — not to kick ϕ too far away from the value inferred from observations, we require:

$$H_{\rm rh} \ll 2\pi\Delta\phi_i\,.$$

(3.26)

For example, choosing the mean values for the DS parameterisation in table 4 for the data combination with Union3, we obtain an upper bound on the reheating scale, $H_{\rm rh} \ll 0.06 M_{\rm Pl}$. We will obtain analog bounds in our model-by-model analyses below.

4 Cosmological analysis

We modify the cosmological Boltzmann code `CAMB` to implement the three hilltop models as well as the DS parameterisation described above. For each model, we perform a Markov Chain Monte-Carlo (MCMC) analysis of the parameter space, varying two model specific parameters (described below) alongside the baseline cosmological parameters $\{\Omega_{\rm b}h^2, \Omega_c h^2, H_0, \tau, A_s, n_s\}$ for which we adopt wide uniform priors. We make use of the following datasets:
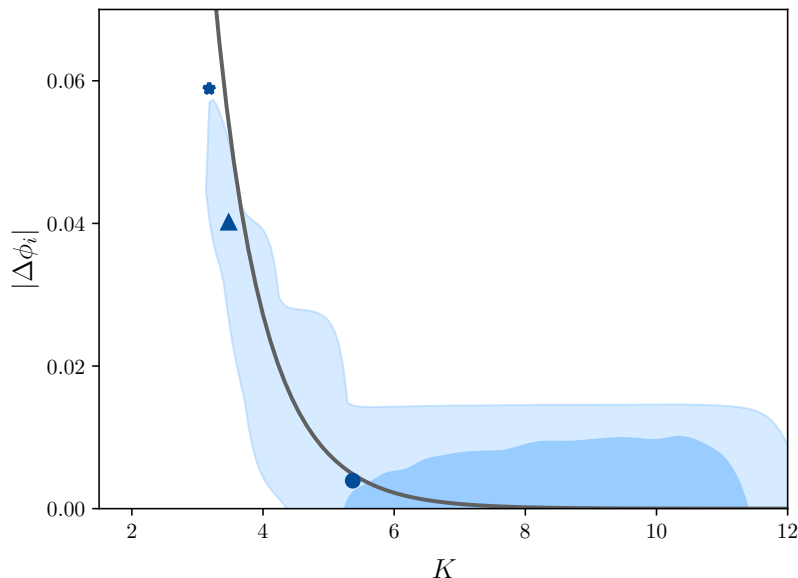
Figure 8. Analytic results for $\Delta\phi_i$ obtained from eq. (3.25) for the hilltop quintessence models, and posterior contours furnished by a MCMC analysis in the K-$|\Delta\phi_i|$ plane. The analytic results are represented in dark grey line using best-fit values for $\Omega_{\phi,0}$ and w_0 from the data combination with Union3. Dark blue shapes indicate the points corresponding to the best-fit values (see tables 6–8) for model parameters (ϕ_0 and f): circle for axion model, star for sugra model and triangle for the field theory model. In the same figure, we show with blue contours the 1σ and 2σ bounds in the $K - |\Delta\phi_i|$ plane from the constraints on the DS parameterisation for the data combination with Union3. See figure 19 in the appendix for the analogous figure including constraints from all the data combinations.

1. CMB from *Planck* 2018:

    - *Planck* 2018 low-ℓ temperature and polarisation likelihood [54].

    - *Planck* high-ℓ CamSpec TTTEEE temperature and polarization likelihood using `NPIPE` (*Planck* PR4) data [55].

    - *Planck* 2018 lensing likelihood [56].

    Hereafter, we collectively refer to all the *Planck* CMB likelihoods as 'CMB'.

2. BAO likelihoods from DESI DR1 [29, 57, 58]

3. Pantheon+ [59], Union3 [60] and DES-Y5 [28] type Ia supernovae likelihoods.

We sample the likelihoods using the `MCMC` sampler [61, 62], provided in `Cobaya` [63]. Our convergence criteria for the MCMC chains is reached at the value $R - 1 = 0.02$ for the Gelman-Rubin diagnostic. The constraints and posterior distribution plots for each model are generated using the `GetDist` package [64]. We also run the `Py-BOBYQA` [65, 66] minimizer via `Cobaya` to obtain the maximum likelihood point and the corresponding χ^2 values.

Recent results from the DESI BAO analysis [29], alone as well as when combined with supernovae data from Pantheon+ [59], Union3 [60] and DESY5 [28], exhibit a preference for dynamical dark energy with a fairly rapid evolution in the recent past [29, 67–69]. The

significance of this deviation from ΛCDM ranges from $2 - 4\sigma$, depending upon the supernovae dataset chosen.[16] When it comes to the quintessence models considered here, these datasets allow us to provide constraints on the underlying model parameters as well as test whether these models can provide a better fit to the data compared to ΛCDM, or to the CPL parameterisation [90–92].

4.1 Axion hilltop

For the axion model discussed in section 2.2 we sample the axion decay constant f and the initial field value θ_i rescaled by f, i.e. θ_i/f, for $f < 2$. The results are plotted in figure 9 and 68% limits summarised in table 1 for the parameters[17] $\{f, \theta_i/f, \Omega_b h^2, \Omega_c h^2, H_0\}$. Focusing on the 1D marginalised constraints for the parameter f, we notice a preference for larger ($f \gtrsim 1$) values in the Pantheon+ dataset, which decreases progressively as we change the supernovae dataset to Union3 or DESY5. In addition, from the constraints in the (f-θ_i/f) plane using the DESY5 SN dataset, we learn that for smaller f, the allowed values of θ_i/f are squeezed to a small region around π, while for larger f the region around $\theta_i/f = \pi$ is excluded. This happens because for larger f (smaller slope), one has to start farther away from the hilltop (maxima) to obtain dynamical dark energy at the present epoch. These effects are much less pronounced for the other SN datasets, reflecting the fact that these do not deviate from ΛCDM as much as DESY5. In other words, for the DESY5 dataset, the preferred field evolution in the axion model requires either the field starting far away from the maximum, if f is large, or the field starting close to the maximum, if f is small.

Table 1 indicates that the combined data sets give a lower bound on f at around $f \gtrsim 0.7$ (68% C.L), and including the DESY5 data gives a mean value $f = 0.88^{+0.24}_{-0.54}$. Note that the lower-limits and means presented here derive from a Bayesian analysis of the model against the cosmological data, thus they are highly prior-dependent. As we can see in both figure 9 and table 1, the data are not particularly constraining when it comes to the parameters $f, \theta_i/f$ and — as long as this is the case — the prior dependence of the limits is expected to remain. On the other hand, refinement of the theory priors on f (or even θ_i) will lead to tighter constraints on these parameters. If evidence for dynamical dark energy persists, the parameter region $f > 1$ with θ_i close to the maximum will be strongly disfavoured.

Motivated by the swampland constraints discussed in section 2, which suggest $f \lesssim \mathcal{O}(1)M_{\rm Pl}$, we have assumed the prior that $f < 2M_{\rm Pl}$, restoring Planck units. It would be important to refine the order one constants that appear in the swampland constraints. Nevertheless, the values of f favoured by our analysis are rather large from the string theory point of view and they could only be pushed further up by extending the priors to allow larger values for f, until the data is sufficiently constraining to make the fits prior-independent. In particular, for such large values of[18] $f \gtrsim 0.7M_{\rm Pl}$, the weak gravity conjecture (2.2) implies

---

[16]Different interpretations of these results as well as their various cosmological implications are also discussed in [70–89].

[17]For each model studied in this section, the results for the full set of parameters including the best-fit parameter combinations are presented in appendix B. In this section, we focus mainly on the dark energy model specific and the cosmological background parameters as, in any case, the constraints on the other cosmological parameters do not differ significantly across the different models or the different datasets.

[18]Large values of f also imply large values for θ_i in Planck units. The distance conjecture [50] generally puts

Parameter	+Pantheon+	+Union3	+DESY5
f	> 0.946	> 0.779	$0.88^{+0.24}_{-0.54}$
θ_i/f	—	—	< 2.62
$\Omega_c h^2$	0.11842 ± 0.00081	0.11842 ± 0.00083	0.11847 ± 0.00086
$\Omega_b h^2$	0.02227 ± 0.00012	0.02227 ± 0.00013	0.02227 ± 0.00013
H_0	$67.49^{+0.51}_{-0.37}$	$67.23^{+0.81}_{-0.40}$	$66.79^{+0.74}_{-0.62}$
θ_i	$3.1^{+1.1}_{-1.4}$	$2.73^{+0.93}_{-1.6}$	$2.11^{+0.40}_{-1.2}$

Table 1. Axion model: parameter means and 68% limits for the addition of the different supernovae datasets to the CMB+DESI combination.

that the instanton that generates the scalar potential has action $S_{\text{inst}} \lesssim 1.4$. This means that an additional source of exponential suppression is needed to achieve the hierarchically small scale of Dark Energy — e.g. in the form of polyinstantons as discussed in [93, 94]. Recalling also that control of the instanton expansion requires $S_{\text{inst}} \gtrsim 1$, theoretical and observational constraints combine to give a very narrow window of possibilities that would have to rely on numerical control.

Finally, it is interesting to consider the implications of the observational constraints on the initial conditions for the inflationary or reheating scale, by demanding that the initial conditions are safe from quantum diffusion at the time of reheating. Following section 3.4, and using the mean values for θ_i and f from the CMB+DESI+DESY5 data in table 1 for illustration, we find, restoring M_{Pl}:

$$H_{\text{rh}} \ll 2\pi(\pi f - \theta_i) = 4.1 M_{\text{Pl}}, \tag{4.1}$$

that is, there is no effective constraint on the reheating scale.

Note that the axion model has been analysed previously in [95], using the cosmological data available at that time. Our results with the new datasets are in agreement with their results, with the slight differences in the constraints on the axion parameters mainly driven by the new datasets.

4.2 Saxion hilltop

For the saxion model we sample the parameter $\alpha \in \left(\frac{2\pi}{32}, \frac{2\pi}{9}\right)$, consistent with our theory discussion in section 2, and the initial field value ϕ_i, rescaled by ϕ_{max}, i.e. ϕ_i/ϕ_{max}. The results are plotted in figure 10 and the 68% limits summarised in table 2 for the parameters $\{\alpha, \phi_i/\phi_{\text{max}}, \Omega_b h^2, \Omega_c h^2, H_0\}$.

We interpret these parameter constraints in terms of the series expansion of the Saxion potential in (3.21), where we learn that α effectively plays the role of the potential's curvature through the term ϕ_{max}. Since the field value at the potential maximum is a function of

super-Planckian field ranges in the swampland, but, in our hilltop scenario, the field range actually explored would be small due to Hubble friction.
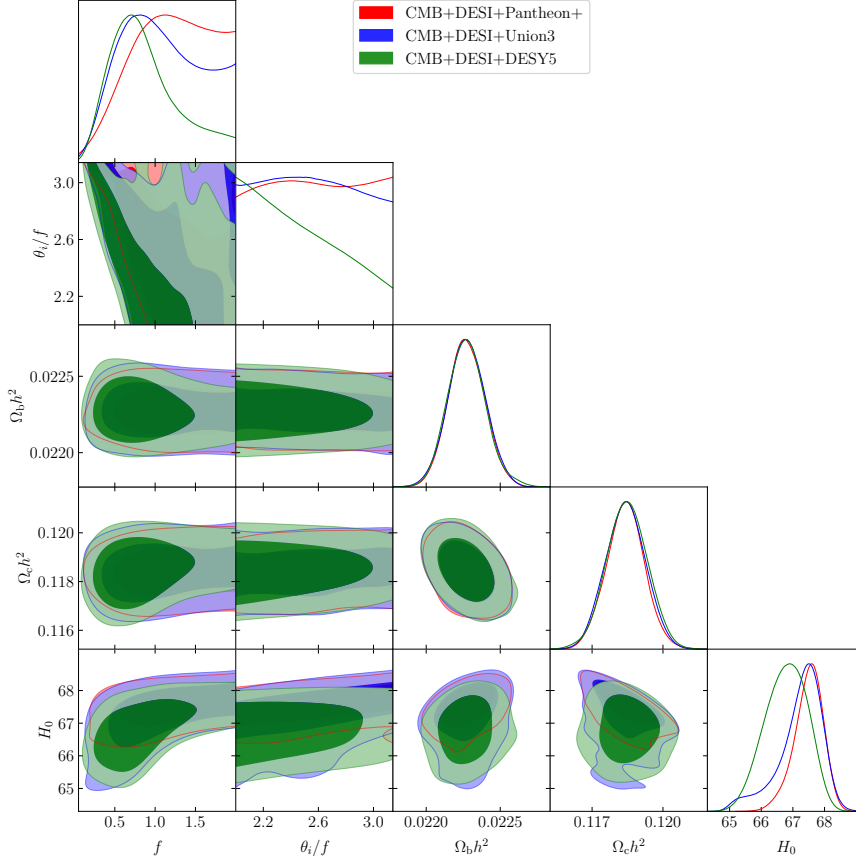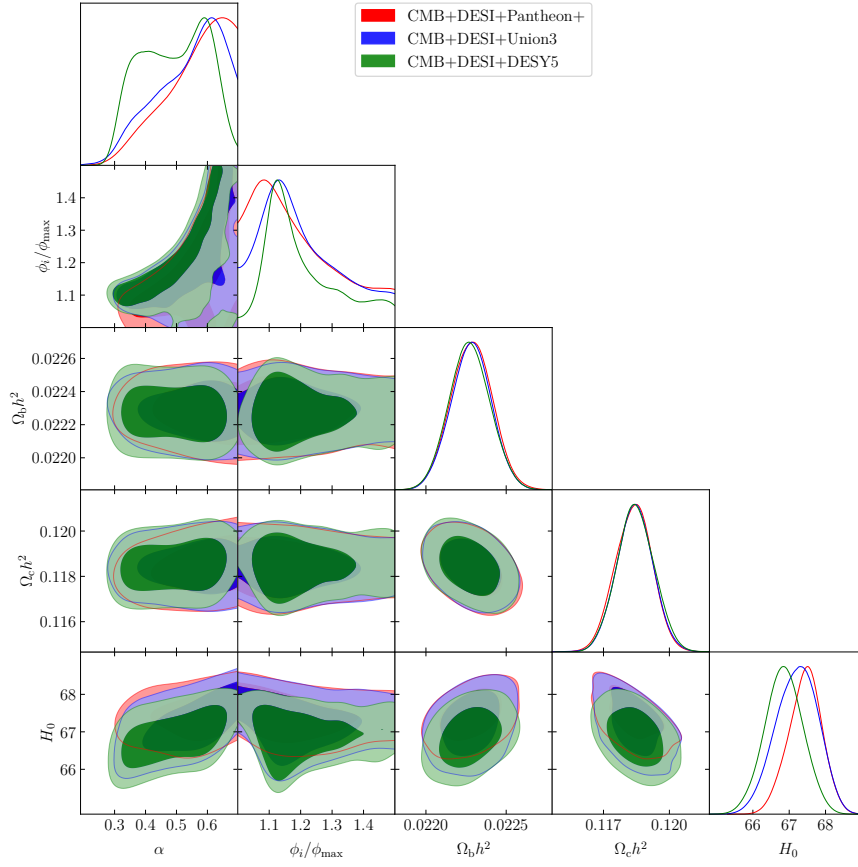
Figure 9. Parameter constraints on the Axion model, eq. (2.1) (68% and 95% contours).

α (2.4), the potential has a higher curvature for smaller α and lower curvature for larger α. Thus, for smaller α the parameter $\phi_i/\phi_{\max}$ is constrained to be close to one. This manifests as a somewhat curved degeneracy in the α–$\phi_i/\phi_{\max}$ plane in figure 10. Focusing in particular on the DESY5 contours (green), whilst $\phi_i/\phi_{\max}$ moves towards smaller values as α decreases, it cannot be too close to 1 as otherwise one would not obtain dynamical dark energy at the present epoch, as is preferred by the DESY5 data. Although current data do not put any tight constraint on the fundamental parameter α, if e.g. ϕ_i is forced to be closer to the hilltop and upcoming surveys continue to see evidence for dynamical dark energy, the preferred region for α would be driven towards lower values.

Finally, we note the constraints on the reheating scale, by demanding that the initial conditions are safe from quantum diffusion at that time. Following section 3.4, and using the mean values for ϕ_i and α from the CMB+DESI+DESY5 data in table 2 for illustration, we find, restoring $M_{\rm Pl}$:

$$H_{\rm rh} \ll 2\pi \left(\phi_i - \frac{1}{\sqrt{2}} \log \left(\frac{1}{\sqrt{2}\alpha} \right) \right) = 0.38 M_{\rm Pl} \,. \tag{4.2}$$

Figure 10. Parameter constraints (68% and 95% contours) for the Saxion model (2.3).

Parameter	+Pantheon+	+Union3	+DESY5
α	> 0.521	$0.537^{+0.16}_{-0.045}$	0.49 ± 0.11
$\phi_i/\phi_{\mathbf{max}}$	< 1.23	$1.201^{+0.071}_{-0.17}$	$1.205^{+0.058}_{-0.14}$
$\Omega_{\mathbf{c}}h^2$	0.11838 ± 0.00084	0.11842 ± 0.00083	0.11846 ± 0.00085
$\Omega_{\mathbf{b}}h^2$	0.02228 ± 0.00013	0.02228 ± 0.00013	0.02228 ± 0.00012
H_0	$67.44^{+0.49}_{-0.43}$	$67.21^{+0.62}_{-0.55}$	66.86 ± 0.52
ϕ_i	$0.209^{+0.064}_{-0.18}$	$0.241^{+0.083}_{-0.21}$	$0.32^{+0.13}_{-0.22}$

Table 2. Saxion model: parameter means and 68% limits for the addition of the different supernovae datasets to the CMB+DESI combination. The full set of constraints can be found in table 7 and corresponding plots in figure 16.

Parameter	+Pantheon+	+Union3	+DESY5
ϕ_0	> 1.29	> 1.24	> 1.17
ϕ_i/ϕ_0	< 0.142	$0.151^{+0.073}_{-0.12}$	0.169 ± 0.081
$\Omega_c h^2$	0.11838 ± 0.00082	0.11835 ± 0.00084	0.11829 ± 0.00084
$\Omega_b h^2$	0.02228 ± 0.00012	0.02228 ± 0.00013	0.02228 ± 0.00013
H_0	$67.29^{+0.59}_{-0.45}$	$66.7^{+1.0}_{-0.70}$	66.44 ± 0.64
ϕ_i	$0.174^{+0.071}_{-0.17}$	$0.235^{+0.088}_{-0.23}$	$0.26^{+0.10}_{-0.24}$

Table 3. Higgs-like hilltop model: parameter means and 68% limits for the addition of the different supernovae datasets to the CMB+DESI combination.

4.3 Higgs-like hilltop

For the Higgs-like hilltop,[19] we vary the parameter ϕ_0 and the initial relative field value ϕ_i/ϕ_0. In fact these two quantities play a role similar to f, θ_i/f in the Axion model, representing the steepness of the potential and the initial displacement from the maximum. The resulting parameter posterior distributions can also be interpreted similarly and are plotted in figure 11, with the 68% limits summarised in table 3. In particular, we notice the same squeezing of the allowed ϕ_i when the potential is steep, i.e. for smaller ϕ_0, as found in the axion model of section 4.1. The limits from the current cosmological data are strongly prior dependent and once again, a more precise understanding of the theoretical priors on ϕ_0 and ϕ_i will be crucial to constraining the parameter space of this model.

Finally, we estimate the constraints on the reheating scale from quantum diffusion and the degree of fine-tuning in the initial conditions that the data indicates. Following section 3.4, and using the mean value for ϕ_i from the CMB+DESI+DESY5 data in table 3 for illustration, we find, restoring $M_{\rm Pl}$:

$$H_{\rm rh} \ll 2\pi\phi_i = 1.6 M_{\rm Pl}\,, \tag{4.3}$$

that is, no effective constraint on the reheating scale.

4.4 DS parameterisation analysis

For the DS parameterisation, we vary the parameters K and w_0 along with the other six CDM parameters as in the previous sections. The results for the posterior probability distributions are plotted in figure 12 and the corresponding 68% limits are presented in the table 4. The full set of posterior distributions and corresponding limits are reported in figure 18 and table 9, respectively. The 1D posterior distributions of K for all data combinations are skewed towards smaller values — as expected since smaller curvature is required when the initial field value is far from the hilltop (see also the discussion around figure 8). For what

---

[19]See [96] for a cosmological analysis of a pure quadratic hilltop.
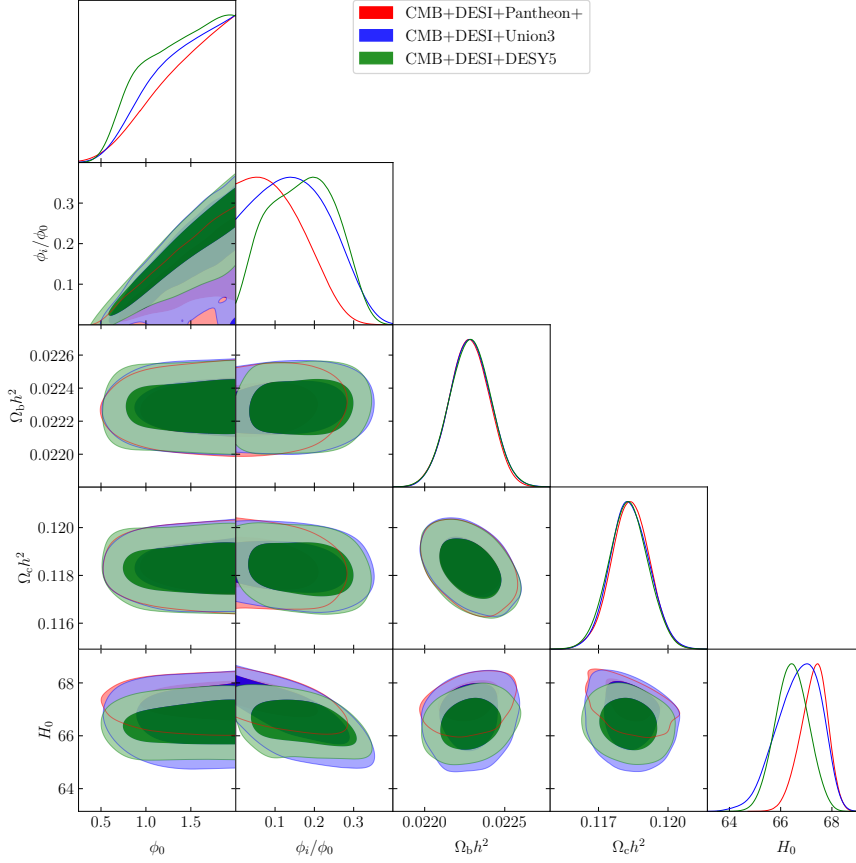
Figure 11. Constraints on the Higgs-like hilltop model (2.5) (68% and 95% contours).

concerns the combination with Pantheon+ results, the large K tail of the 1D posterior is a consequence of the condition $w_0 \simeq -1.0$ being preferred when this data set is added.[20]

Although a one-to-one match among the posteriors of f and ϕ_0 with that of K is not expected due to the non-linear relation between these parameters (3.19), and (3.22) — as well as the complicated mapping between ϕ_i and w_0 — the values of K obtained directly from f and ϕ_0 can nevertheless be compared with the posterior of K from DS parameterisation. Using the mean values for f and ϕ_0 from tables 1 and 3 (for +Union3) leads to $K_{ax}^{mean} < 1.45$, and $K_{Higgs}^{mean} < 2.11$, while $K_{sugra} = 3.179$ is independent of model parameters.[21] However, K in DS parameterisation is not very tightly constrained for any data combination, as compared to its prior range, allowing for the values of K from the individual model constraints to lie within 1σ — 3σ of their DS counterparts, depending on the data combination under consideration. This can also be clearly seen in figure 8 in the relative position of the dots (for model predictions) with respect to the shaded 1σ and 2σ regions in the K-$|\Delta\phi_i|$ plane.

A similar analysis for the DS parameterisation can be found in [52], where a number of parameters including K have been varied, while CDM parameters were kept fixed at CMB

---

[20]Our prior range for w_0 excludes the $w_0 < -1.0$ region.

[21]Using best-fit values for f and ϕ_0 from tables 6 and 8 respectively (for +Union3), viz, $K_{ax}^{best-fit} = 5.3685$, and $K_{Higgs}^{best-fit} = 3.4765$.

Parameter	+Pantheon+	+Union3	+DESY5
K	$7.6^{+2.5}_{-2.1}$	$8.2^{+2.7}_{-1.4}$	$8.4^{+2.4}_{-1.1}$
w_0	< -0.709	$-0.11^{+0.39}_{-0.61}$	$-0.35^{+0.24}_{-0.33}$
$\Omega_c h^2$	0.11830 ± 0.00081	0.11828 ± 0.00086	0.11825 ± 0.00082
$\Omega_b h^2$	0.02226 ± 0.00013	0.02227 ± 0.00013	0.02227 ± 0.00013
H_0	67.53 ± 0.39	66.73 ± 0.59	67.04 ± 0.42

Table 4. DS parameterisation: parameter means and 68% limits for the addition of the different supernovae datasets to the CMB+DESI combination.

values. This analysis obtained even larger values for K, albeit with large error. Our results and those in [52] are consistent within 2σ error.

Finally, we note that w_0 itself is also poorly constrained. Due to the weak constraints on the DS parameters w_0, K, the derived constraints on $|\Delta\phi_i|$ shown in figure 8 also allow for a large range of values. Since w_ϕ is best constrained at around $z \approx 0.4$ — as manifest also from the DESI reconstruction plotted in figure 13 below — we also present the derived constraints on $w_\phi(z = 0.4)$ in figure 20 in appendix B as 2D posterior plots from the analysis of DS parameterisation. In particular, the w_0-$w_\phi(z = 0.4)$ plot demonstrates that the constraints on $w_\phi(z = 0.4)$ are improved by at least an order of magnitude as compared to the constraints on w_0 only.

4.5 Model comparison

To compare the quality of the fit to the data provided by the different models, we perform a model comparison based on the Akaike information criterion (AIC) [97, 98], which also takes into account the number of free parameters of the model. The AIC value is defined as follows

$$\mathrm{AIC} = 2n - 2\ln\mathcal{L}_{\max}, \qquad (4.4)$$

where $\mathcal{L}_{\max}$ stands for the maximum likelihood value in the model and n the number of free parameters. Models with smaller AIC are favoured by the data with the best model having the lowest AIC value. To compare between models, one looks at the difference in AIC values with $\Delta\mathrm{AIC}_{12} \equiv \mathrm{AIC}_1 - \mathrm{AIC}_2 \lesssim 2$ indicating no preference between Model 1 and Model 2, whilst $\Delta\mathrm{AIC}_{12} \gtrsim 5$ indicates a strong preference for Model 2 over Model 1.

The AIC values for the different models we have studied are provided in table 5, where we also consider ΛCDM, the CPL parameterisation and the exponential runaway quintessence model. We learn that the preference for the hilltop quintessence models over ΛCDM is strongest for the dataset combination CMB+DESI+DESY5 and weakest for CMB+DESI+Pantheon+. Out of all the different models studied here, the CPL parameterisation remains the most favoured, irrespective of the dataset combination chosen. However, its improvement with respect to the DS parameterisation is data dependent, with best improvement for +Union3 ($\Delta\mathrm{AIC}_{\mathrm{DS,CPL}} \simeq 8.3$) and only mild improvement for +DESY5 ($\Delta\mathrm{AIC}_{\mathrm{DS,CPL}} \simeq 3.4$). We attribute this improvement to the more rapid evolution of the
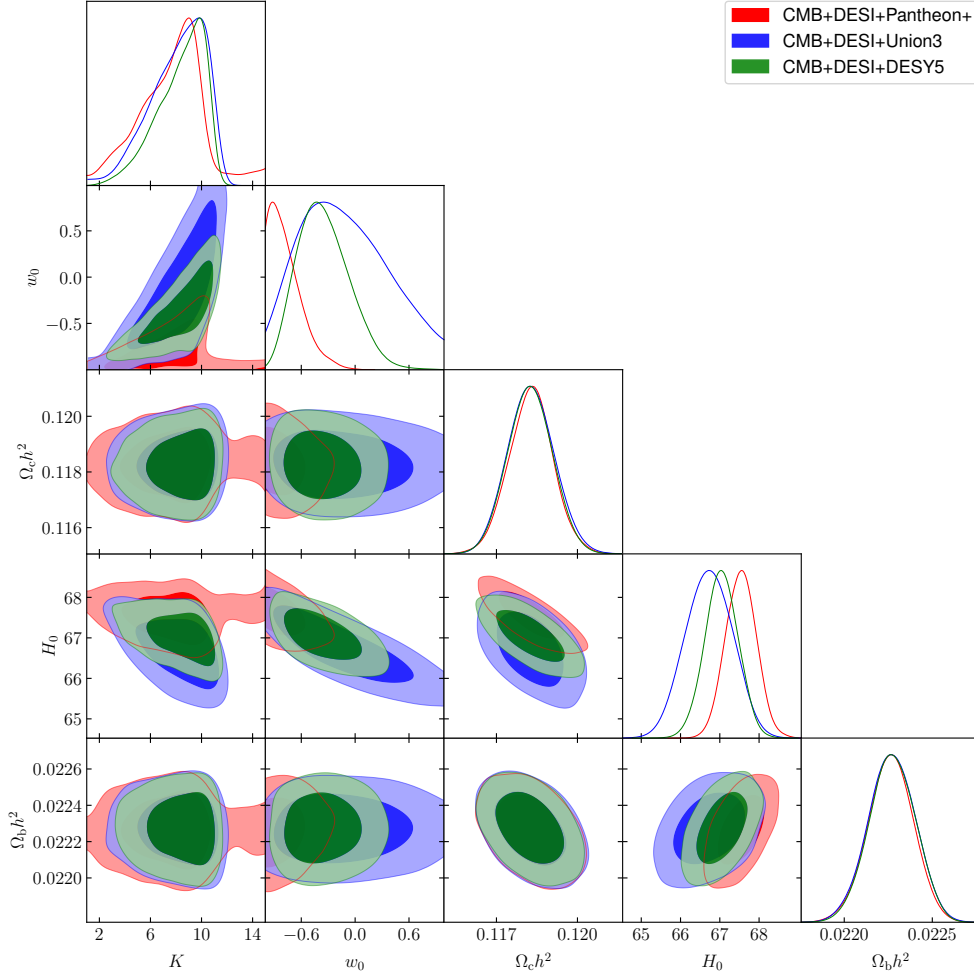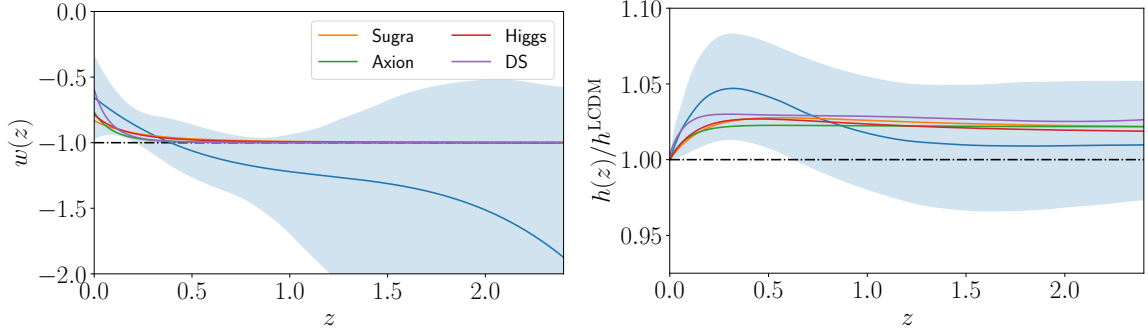
Figure 12. DS parameterisation: parameter means and limits for the addition of the different supernovae datasets to the CMB+DESI combination.

dark energy equation of state in this model, as well as the phantom-like behaviour in the past [29], which matches very well the DESI reconstruction of background quantities $w(z)$ and $h(z) \equiv H(z)/H_0$, shown in figure 13. As is clear from figure 13, these two features cannot be produced in the hilltop quintessence models. On the other hand, the redshift evolution seen here for the hilltop quintessence models is much closer to the DESI reconstruction than what can be produced in the exponential potential model (compare figure 10 of [16]). At the same time, table 5 tells us that the overall improvement in the fit compared to the exponential model is not significant enough to compensate for the additional parameter introduced by the hilltop models.

We also notice that the DS parameterisation fares (marginally) better than the concrete hilltop quintessence models we considered, with the greatest improvement for +DESY5 with $\Delta \mathrm{AIC}_{\mathrm{model,DS}} \simeq 4$, and the lowest improvement for +Pantheon+ with $\Delta \mathrm{AIC}_{\mathrm{model,DS}} \lesssim 0.6$. One can then also adopt the approach to start from the DS parameterisation, compare it with data, and infer the preferred values for the curvature parameter K. We can then use

AIC	Axion	Sugra	Higgs	DS	ΛCDM	CPL	Exp
CMB+DESI+Pantheon+	12409.55	12409.40	12409.07	12408.9	12406.04	12401.70	12407.19
CMB+DESI+Union3	11030.07	11029.49	11030.38	11027.9	11028.69	11019.62	11029.00
CMB+DESI+DESY5	12644.67	12645.65	12644.89	12641.2	12649.01	12637.79	12644.73

Table 5. Comparison between the different models considered in this section.

Figure 13. The quantities $w_\phi(z)$, and $h(z) \equiv H(z)/H_0$ are plotted for the best-fit hilltop models as indicated, and compared to the DESI reconstruction (blue line) using CMB+DESI+Union3 data [67]. The CPL parameterisation matches the DESI reconstruction. The shaded regions represent the 95% confidence regions. At $z = 0$, $w_0 = -0.65$ for the reconstruction, while the values for the hilltop models are as follows $w_0 = -0.77$ for the axion model, $w_0 = -0.83$, for the saxion and $w_0 = -0.79$ for the Higgs-like hilltop. For comparison, $w_0^{\text{exp}} = -0.89$ for the exponential model (see figure 10 of [16]). For the DS parameterisation, the best-fit value is $w_0^{\text{DS}} = -0.60$. The best-fit parameter values for each model can be found in appendix B.

these results to deduce a preference for specific hilltop scenarios, given that each model favours its own preferred range of K, depending on each model parameters. The evolution of the background parameters plotted in figure 13 shows clearly that the DS parameterisation tracks the predictions from hilltop quintessence models well until very low redshift, $z \gtrsim 0.1$, beyond which it leads to a faster evolution of $w(z)$.

5 Outlook and future challenges

Embedding models of dark energy in quantum gravity and string theory is a notoriously difficult task, given stringent theoretical constraints on model building associated with quantum gravity conjectures, as well as strong phenomenological constraints on light fields. At the same time, recent and forthcoming cosmological results are going to probe the behaviour of dark energy with an ever-increasing degree of precision, offering the concrete possibility to test our understanding of dark energy in quantum gravity with cosmological data.

With the aim of exploiting such opportunities, in this work we considered a class of dark energy models — hilltop quintessence — which is able to satisfy theoretical bounds from de Sitter and other quantum gravity conjectures. We examined various realisations of quintessence hilltops based on axions, their supersymmetric partners, and Higgs-like string

embeddings. Axion hilltops are widely considered and particularly well-motivated, as their shift symmetry evades problems with UV sensitivities, fifth-forces and time-variation of fundamental constants, and a priori — at the hilltop — they can be consistent with the weak gravity conjecture. Moreover, we have presented a dynamical mechanism by which hilltop initial conditions could be set up. However, it is important to point out that none of our scenarios solve the cosmological constant problem, hence from a theoretical viewpoint they are at least as fine-tuned as the ΛCDM model.

We studied the cosmological consequences of our three string-motivated hilltop models and discussed a convenient parameterisation of their associated equation of state. We then tested their predictions by means of a Bayesian MCMC analysis with recent CMB, galaxy surveys, and supernova data. We showed to what extent current data can distinguish amongst hilltop models and impose constraints on their parameters. Interestingly, such experimental results are complementary to theoretical bounds from quantum gravity conjectures, and we discussed the consequences of these features for our current understanding of dark energy in string theory. Notably, observational constraints on the axion decay constant for axion hilltop quintessence are in tension with the weak gravity conjecture, illustrating how synergies between constraints from observations and from quantum gravity can rule out otherwise well-motivated models. So far, model comparisons favour the CPL parameterisation over any of our hilltops, ΛCDM, and exponential runaways.[22] However CPL is only mildly improved with respect to the DS parametrisation, especially for the dataset CMB+DESI+DESY5. At the same time, the limited constraining power of current data means that the model parameter constraints and comparisons that we obtained are sensitive to our priors, which are based on theoretical assumptions about viable regions of parameter space. Consequently, given that our inference from cosmological data strongly depends on theoretical assumptions, it is imperative to refine our theoretical understanding of the priors, so as to maximize the informative power of current and forthcoming cosmological datasets for testing dark energy scenarios in quantum gravity. In doing so, we can also hope that this endeavor will inspire new ideas and perspectives for tackling fundamental theoretical challenges, such as the cosmological constant problem in quantum gravity.

Assumptions entering into theoretical priors constrain the size and location of the allowed region in parameter space associated with a given model. This includes the possible values of parameters entering in the model Lagrangian and the allowed initial conditions or field ranges associated with the dynamics of the quintessence scalar. Such information can be theoretically refined by better specifying the 'order one' constants[23] entering the de Sitter conjecture in the inequalities (1.1) and the weak gravity conjecture in (2.2), or by embedding hilltop quintessence into more complete early universe models, able to accurately specify their initial conditions. Also, the range of allowed priors can be limited by enriching the hilltop models to include additional Standard Model matter fields: then, one should take into account further constraints on the parameter space from limits on fifth forces and the time variation of fundamental constants. All these theoretical questions can be addressed by

---

[22]See e.g. [99] for possible maps of the CPL parameterisation to physical quintessence or barotropic dark energy models, though no quintessence potential will give rise to the phantom behaviour seen in figure 13.

[23]See e.g. [13, 100] for work towards fixing these order one constants using dimensional reduction.

developments of the current theoretical tools at our disposal. We believe that such questions are very timely, and addressing them will allow us to exploit the synergy between theory and observations offered by current and forthcoming cosmological probes. We look forward to continuing this analysis in forthcoming publications.

Acknowledgments

A   Saxion-axion stringy hilltops

In this appendix we summarise the saxionic hilltop potential we consider in the main text (2.3). More details can be found in [44] (see also [14]). We also provide a concrete example where the minima of stringy axions can become maxima upon turning on further subleading corrections, thus providing a possible dynamical mechanism that tunes the initial conditions of the axion to the hilltop.

A.1   Saxion hilltops

The model considers some inflationary early Universe scenario that ends in a supersymmetric Minkowski minimum, where most of the string moduli are stabilised and heavy, except for a flat direction corresponding to a chiral superfield Φ. The Kähler potential for such flat direction takes the form:

$$K = -n \ln \left(\Phi + \bar{\Phi} \right), \tag{A.1}$$

where n takes different values depending on the type of modulus. As we will see, we are interested in $n = 1$, which may correspond to some (non-overall) volume modulus, or a complex structure modulus, or the dilaton. The superpotential is given by non-perturbative effects which lift the flat direction at some scale before BBN. The leading term in the non-perturbative superpotential is then given by

$$W_{\rm np} = Ae^{-\alpha\,\Phi}. \tag{A.2}$$

Here α is a constant that can arise from different instanton types or gaugino condensation and can e.g. take values $\alpha = 2\pi/N$, with $N = 1$ for an Euclidean D3-brane instanton and

$N \geq 2$ for gaugino condensation with condensing group rank SU(N). The scalar potential can then be computed using the supergravity formula

$$V = e^K \left[K^{i\bar{j}} D_j W D_{\bar{j}} \bar{W} - 3|W|^2 \right] , \tag{A.3}$$

where $D_j W \equiv \partial_j W + K_j W$. Writing the complex scalar field component of the chiral superfield as $\Phi = \varphi + i\theta$, we obtain:

$$V = \frac{A^2}{2^n n} e^{-2\alpha\varphi} \varphi^{-n} \left(n^2 + n(-3 + 4\alpha\varphi) + 4\alpha^2\varphi^2 \right) , \tag{A.4}$$

which, for $n = 1$, has a dS maximum at:

$$\varphi_{\max} = \frac{1}{\sqrt{2}\alpha} . \tag{A.5}$$

Notice that at the leading order considered, the axion θ remains a flat direction, but it will be lifted by subleading non-perturbative terms [44]. Indeed, adding a subleading contribution

$$W_{\mathrm{np\,sub}} = Be^{-\beta\Phi} \tag{A.6}$$

to the leading contribution (A.2), will generate a minimum for the axion, whilst preserving the (slightly shifted) maximum in the saxion direction, with $|m^2_{\mathrm{axion}}| < |m^2_{\mathrm{saxion}}|$. For example for $n = 1$, $\beta = 2\alpha$, $B = -A/20$, the axion has a minimum at $\theta = \frac{2m\pi}{\beta - \alpha}$, $m \in \mathbb{Z}$ [44]. Note that the exponential suppression of the subleading non-perturbative term is only by a factor $\sqrt{2}$ at the hilltop, so control of the expansion in non-perturbative effects can be at best numerical there. It is useful to express the potential in terms of the canonically normalised field, which for $n = 1$, is

$$\phi = M_{\mathrm{Pl}} \sqrt{\frac{1}{2}} \log \varphi . \tag{A.7}$$

The final potential becomes (2.3).

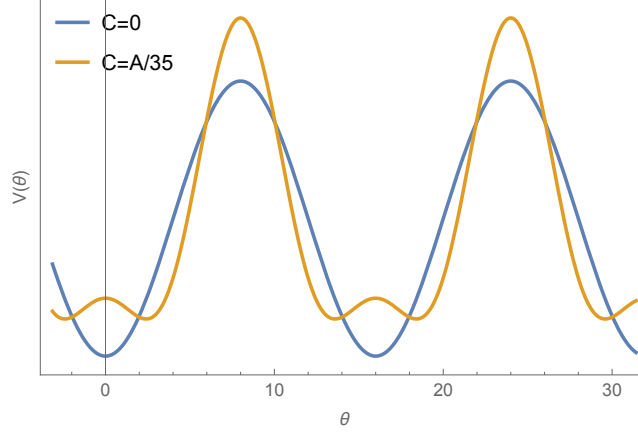## A.2 Subleading corrections to the axion

Let us focus on the axion in the model considered above. As we saw, the axion is lifted after adding subleading correction (A.6). Now further subleading corrections of the form

$$W_{\mathrm{sub\,sub}} = Ce^{-\gamma\Phi} , \tag{A.8}$$

may turn the minimum of the axion potential at $C = 0$ into a maximum when $C \neq 0$. This will happen for suitable values of the parameters α, β, γ, and A, B, C. Schematically, the potential (A.3) including the two subleading corrections, (A.6), (A.8) takes the form

$$V = g(\varphi_0) + f_1(\varphi_0) AB \cos\left((\beta - \alpha)\theta\right) + f_2(\varphi_0) AC \cos\left((\gamma - \alpha)\theta\right) + f_3(\varphi_0) BC \cos\left((\gamma - \beta)\theta\right) , \tag{A.9}$$

where $g(\varphi_0), f_i(\varphi_0)$ are functions of the saxion (as well as α, β, γ) evaluated at its extremum. For the case $C = 0$ and $B < 0$, as discussed above, the potential has a minimum at $\theta_{\min} = \frac{2m\pi}{\beta - \alpha}$. When C is turned on, this minimum can become a maximum for suitable values of the parameters. For example, for $n = 1$ as above, $\alpha = 2\pi/16$, $\beta = 2\alpha$, $\gamma = 3\alpha$, $B = -A/20$, $C = A/35$ ($A = 1$ for concreteness), the minima for the axion at $C = 0$ become maxima for $C \neq 0$. It is also possible that some minima stay minima, while only some become maxima. Of course, more complex modulated structures can arise.

Figure 14. Subleading corrections to axion potential (A.9) (in arbitrary units) as described in the text for $(A, B, C) = (1, -A/20, A/35)$, $(\alpha, \beta, \gamma) = (2\pi/16, 2\alpha, 3\alpha)$. The minima become a maxima when the subleading correction is turned on.

## B Constraints for all the parameters of our models

In this section we present the plots and tables with the full set of parameters for the three hilltop models we considered in the main text, as well as the Dutta-Scherrer (DS) parameterisation.

B.1 Axion hilltop

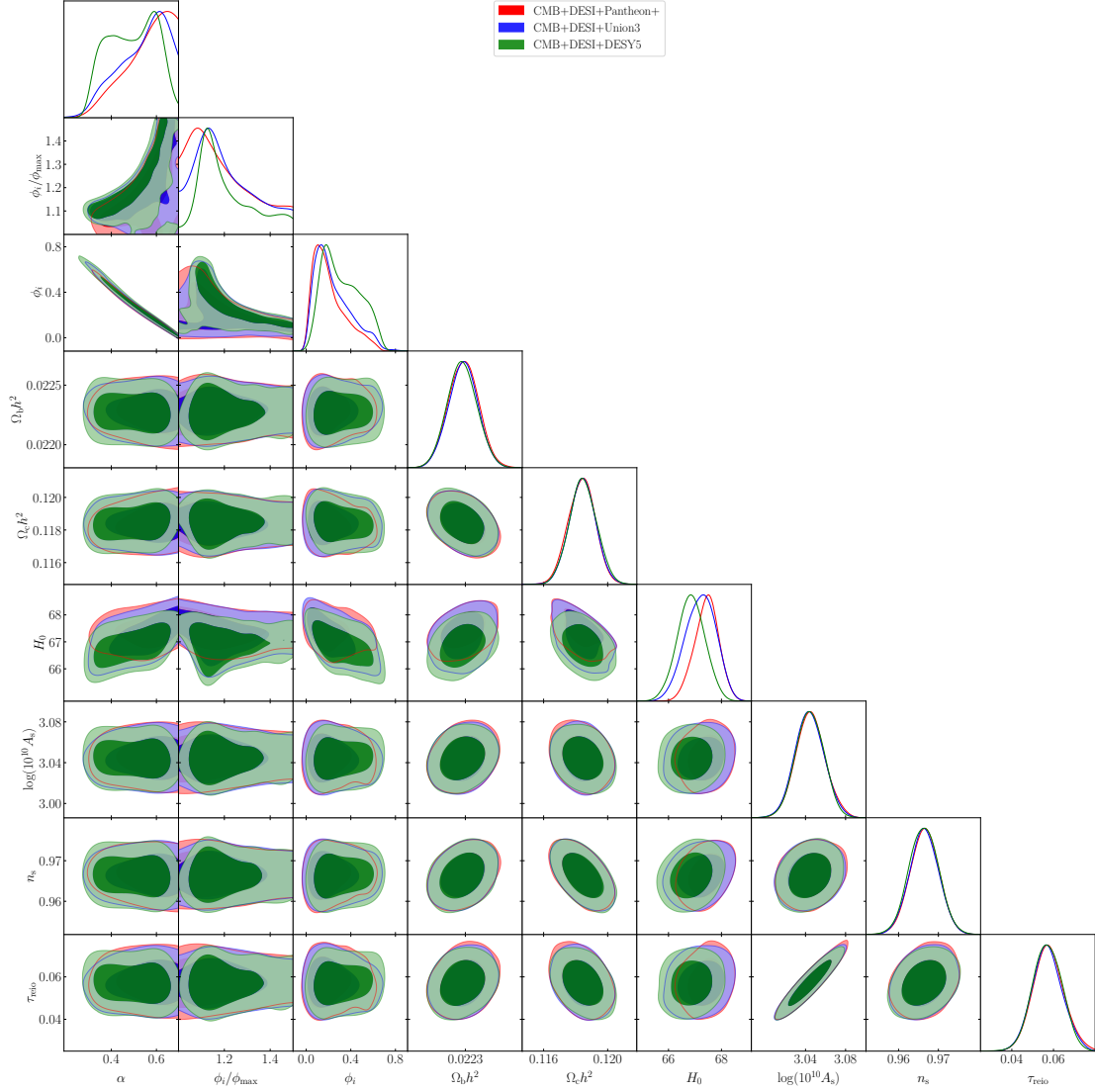| Parameter	+Pantheon+	+Union3	+DESY5
f	$> 0.946 \, {\scriptstyle (1.22)}$	$> 0.779 \, {\scriptstyle (0.15)}$	$0.88^{+0.24}_{-0.54} \, {\scriptstyle (0.19)}$
θ_i/f	$- \, {\scriptstyle (2.25)}$	$- \, {\scriptstyle (3.12)}$	$< 2.62 \, {\scriptstyle (3.07)}$
$\Omega_c h^2$	$0.11842 \pm 0.00081 \, {\scriptstyle (0.11184)}$	$0.11842 \pm 0.00083 \, {\scriptstyle (0.118)}$	$0.11847 \pm 0.00086 \, {\scriptstyle (0.118)}$
$\log(10^{10} A_s)$	$3.045 \pm 0.014 \, {\scriptstyle (3.046)}$	$3.044 \pm 0.015 \, {\scriptstyle (3.048)}$	$3.045 \pm 0.014 \, {\scriptstyle (3.053)}$
n_s	$0.9664 \pm 0.0036 \, {\scriptstyle (0.9647)}$	$0.9664 \pm 0.0037 \, {\scriptstyle (0.9624)}$	$0.9663 \pm 0.0037 \, {\scriptstyle (0.967)}$
H_0	$67.49^{+0.51}_{-0.37} \, {\scriptstyle (67.35)}$	$67.23^{+0.81}_{-0.40} \, {\scriptstyle (66.24)}$	$66.79^{+0.74}_{-0.62} \, {\scriptstyle (65.95)}$
$\Omega_b h^2$	$0.02227 \pm 0.00012 \, {\scriptstyle (0.02223)}$	$0.02227 \pm 0.00013 \, {\scriptstyle (0.0221)}$	$0.02227 \pm 0.00013 \, {\scriptstyle (0.0226)}$
τ_{reio}	$0.0573^{+0.0066}_{-0.0074} \, {\scriptstyle (0.0592)}$	$0.0568^{+0.0067}_{-0.0076} \, {\scriptstyle (0.0586)}$	$0.0573 \pm 0.0071 \, {\scriptstyle (0.061)}$
θ_i	$3.1^{+1.1}_{-1.4} \, {\scriptstyle (2.75)}$	$2.73^{+0.93}_{-1.6} \, {\scriptstyle (0.483)}$	$2.11^{+0.40}_{-1.2} \, {\scriptstyle (0.591)}$

Table 6. Axion model: full parameter means and 68% limits for the addition of the different supernovae datasets to the CMB+DESI combination. The values in parentheses denote the best-fit parameters for this model.
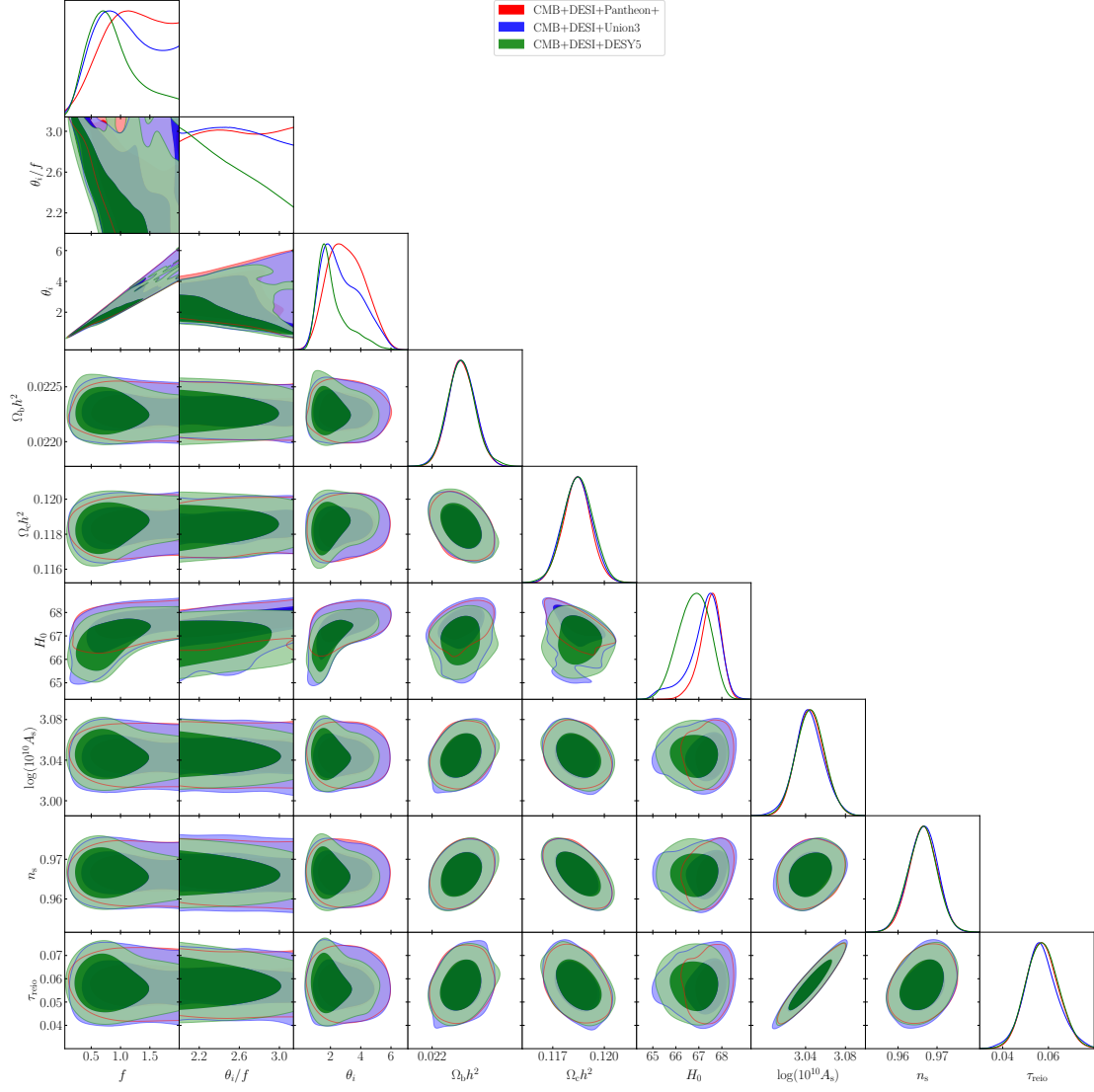
Figure 15. The complete parameter constraints for the Axion model.

B.2 Saxion hilltop

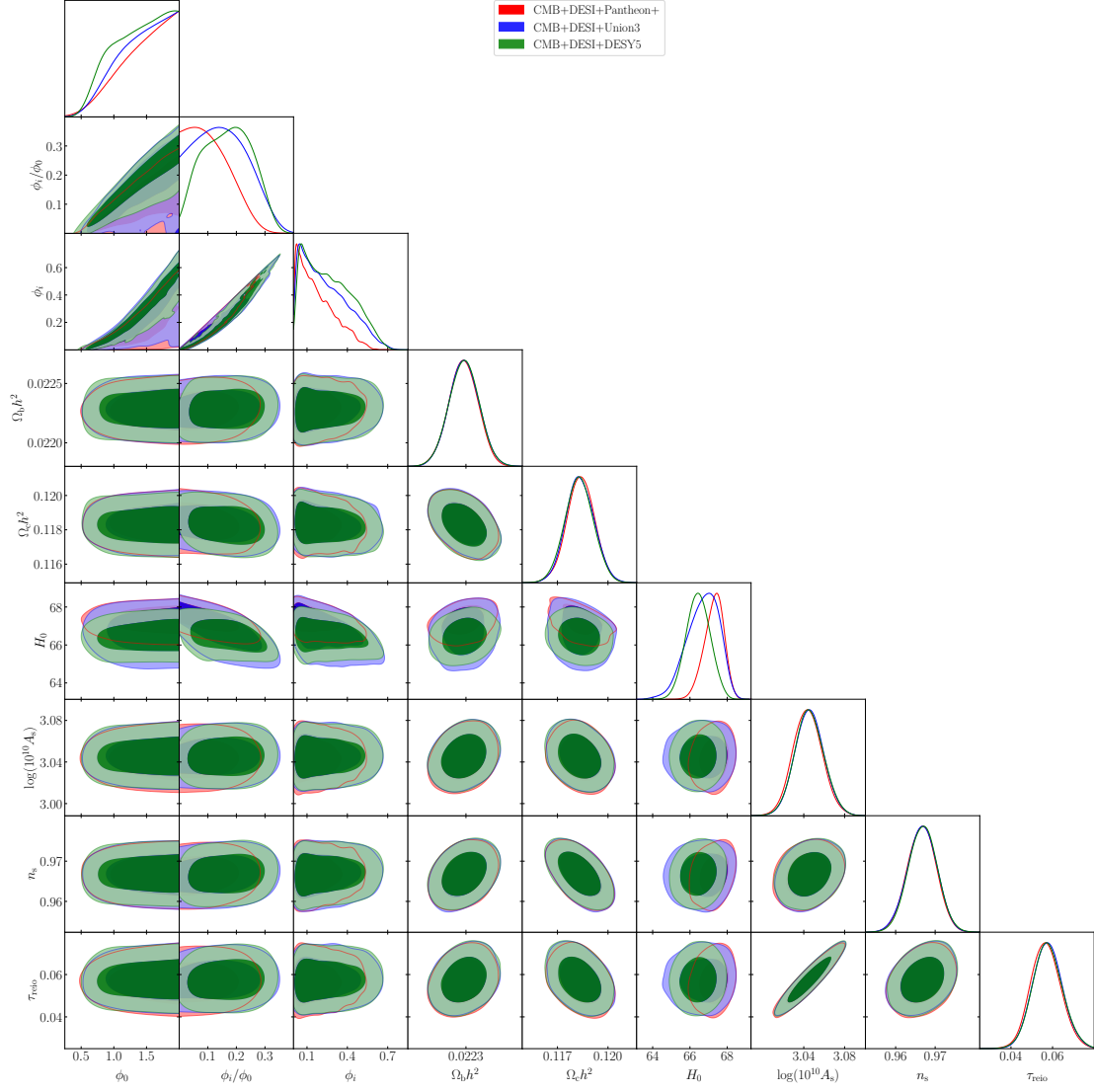**Figure 16.** Full parameter constraints for Saxion model.

Parameter	+Pantheon+	+Union3	+DESY5
α	$> 0.521\,(0.66)$	$0.537^{+0.16}_{-0.045}\,(0.366)$	$0.49 \pm 0.11\,(0.311)$
ϕ_i/ϕ_{max}	$< 1.23\,(1.43)$	$1.201^{+0.071}_{-0.17}\,(1.14)$	$1.205^{+0.058}_{-0.14}\,(1.10)$
$\Omega_c h^2$	$0.11836 \pm 0.00084\,(0.1184)$	$0.11841 \pm 0.00083\,(0.1181)$	$0.11841 \pm 0.00085\,(0.1175)$
$\Omega_b h^2$	$0.02228 \pm 0.00013\,(0.02228)$	$0.02228 \pm 0.00012\,(0.02223)$	$0.02228 \pm 0.00013\,(0.02231)$
$\log(10^{10}A_s)$	$3.045 \pm 0.014\,(3.040)$	$3.044 \pm 0.014\,(3.048)$	$3.044 \pm 0.014\,(3.045)$
n_s	$0.9665 \pm 0.0037\,(0.9650)$	$0.9664 \pm 0.0037\,(0.9644)$	$0.9664 \pm 0.0037\,(0.9665)$
H_0	$67.44^{+0.49}_{-0.43}\,(67.61)$	$67.21^{+0.62}_{-0.55}\,(66.16)$	$66.86 \pm 0.52\,(66.31)$
τ_{reio}	$0.0573 \pm 0.0070\,(0.0552)$	$0.0568^{+0.0067}_{-0.0075}\,(0.0574)$	$0.0572^{+0.0066}_{-0.0076}\,(0.0572)$
ϕ_i	$0.209^{+0.064}_{-0.18}\,(0.07)$	$0.241^{+0.083}_{-0.21}\,(0.53)$	$0.32^{+0.13}_{-0.22}\,(0.64)$

Table 7. Saxion model: full parameter means and 68% limits for the addition of the different supernovae datasets to the CMB+DESI combination. The values in parentheses denote the best-fit parameters for this model.

B.3 Higgs-like hilltop

Parameter	+Pantheon+	+Union3	+DESY5
ϕ_0	$> 1.29\,(1.23)$	$> 1.24\,(0.69)$	$> 1.17\,(0.62)$
ϕ_i/ϕ_0	$< 0.142\,(0.106)$	$0.151^{+0.073}_{-0.12}\,(0.051)$	$0.169 \pm 0.081\,(0.034)$
$\Omega_c h^2$	$0.11838 \pm 0.00082\,(0.1188)$	$0.11835 \pm 0.00084\,(0.1176)$	$0.11829 \pm 0.00084\,(0.1189)$
$\Omega_b h^2$	$0.02228 \pm 0.00012\,(0.02221)$	$0.02228 \pm 0.00013\,(0.00223)$	$0.02228 \pm 0.00013\,(0.02223)$
$\log(10^{10}A_s)$	$3.044 \pm 0.014\,(3.041)$	$3.046 \pm 0.014\,(3.044)$	$3.045 \pm 0.014\,(3.033)$
n_s	$0.9666 \pm 0.0036\,(0.9641)$	$0.9667 \pm 0.0037\,(0.9694)$	$0.9669 \pm 0.0036\,(0.9645)$
H_0	$67.29^{+0.59}_{-0.45}\,(66.98)$	$66.7^{+1.0}_{-0.70}\,(66.30)$	$66.44 \pm 0.64\,(66.06)$
τ_{reio}	$0.0567 \pm 0.0071\,(0.0555)$	$0.0576 \pm 0.0071\,(0.056)$	$0.0576 \pm 0.0072\,(0.0514)$
ϕ_i	$0.174^{+0.071}_{-0.17}\,(0.1313)$	$0.235^{+0.088}_{-0.23}\,(0.0035)$	$0.26^{+0.10}_{-0.24}\,(0.0021)$

Table 8. Higgs-like model: full parameter means and 68% limits for the addition of the different supernovae datasets to the CMB+DESI combination. The values in parentheses denote the best-fit parameters for this model.

**Figure 17.** Full parameter constraints for the Higgs-like model.
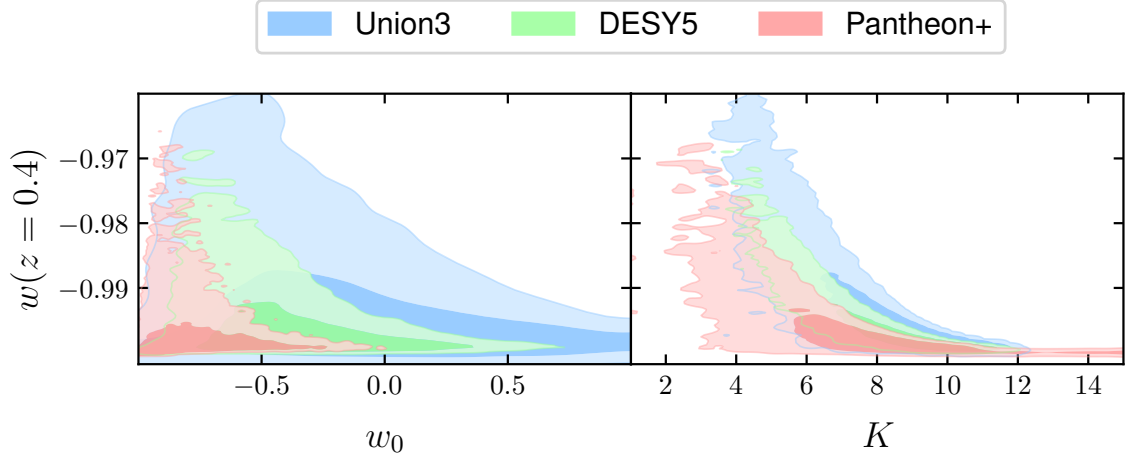
B.4 Dutta-Scherrer parameterisation
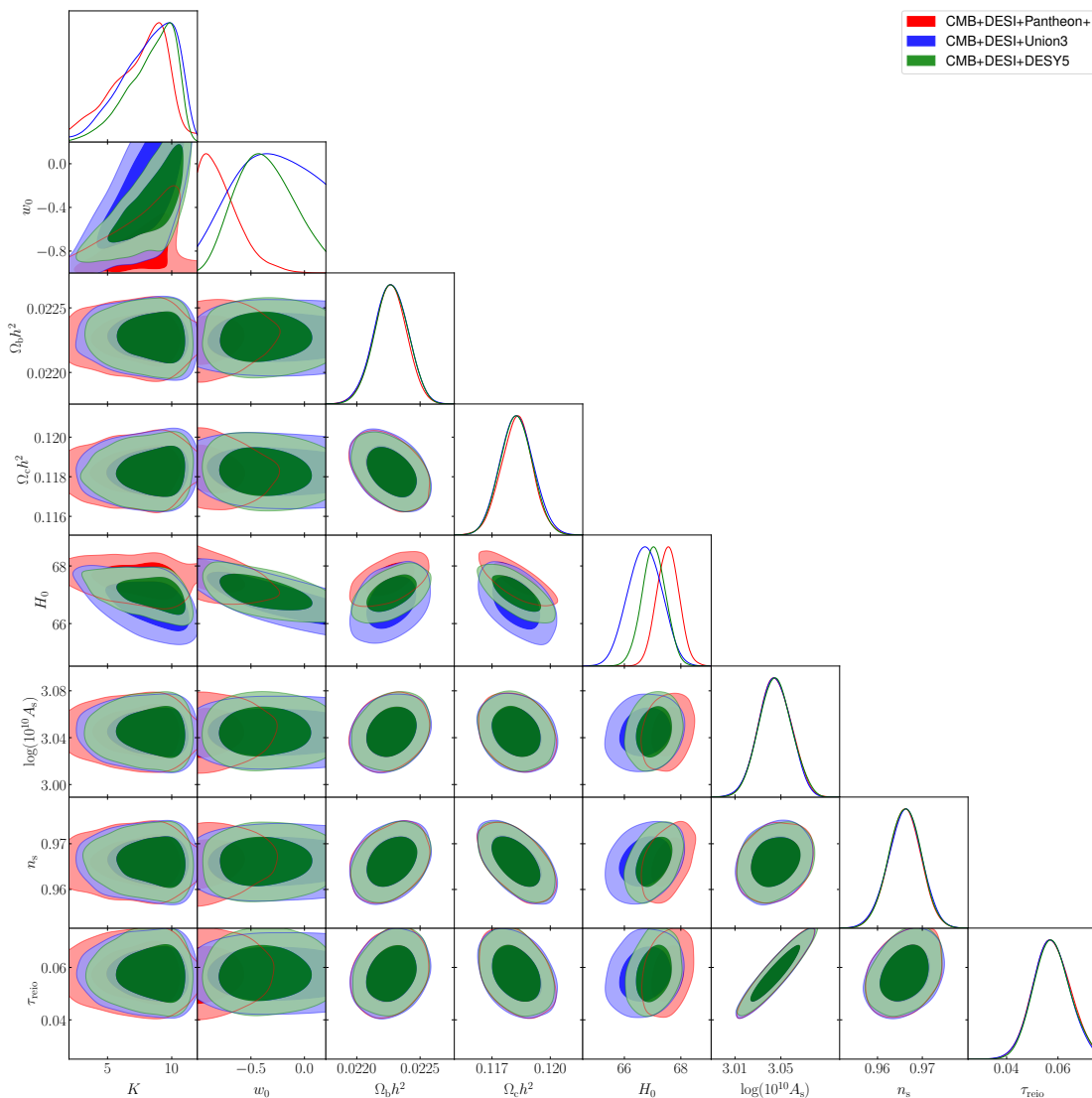
Figure 18. Full parameter plots for the DS parameterisation.

Parameter	+Pantheon+	+Union3	+DESY5
K	$7.6^{+2.5}_{-2.1}$ (7.49)	$8.2^{+2.7}_{-1.4}$ (6.16)	$8.4^{+2.4}_{-1.1}$ (9.52)
w_0	< -0.709 (-0.79)	$-0.11^{+0.39}_{-0.61}$ (-0.60)	$-0.35^{+0.24}_{-0.33}$ (-0.21)
$\Omega_c h^2$	0.11830 ± 0.00081 (0.11782)	0.11828 ± 0.000856 (0.11815)	0.11825 ± 0.00082 (0.11757)
$\Omega_b h^2$	0.02226 ± 0.00013 (0.02228)	0.02227 ± 0.00013 (0.02229)	0.02227 ± 0.00013 (0.02230)
H_0	67.53 ± 0.39 (67.76)	66.73 ± 0.59 (65.92)	67.04 ± 0.42 (67.23)
$\log(10^{10} A_s)$	3.045 ± 0.014 (3.046)	3.044 ± 0.014 (3.045)	3.045 ± 0.014 (3.043)
n_s	0.9659 ± 0.0037 (0.9687)	0.9661 ± 0.0037 (0.9676)	0.9661 ± 0.0036 (0.9665)
τ_{reio}	0.0574 ± 0.0071 (0.0588)	0.0573 ± 0.0070 (0.0580)	0.0576 ± 0.0069 (0.0565)

Table 9. DS parameterisation: full parameter means and 68% limits for the addition of the different supernovae datasets to the CMB+DESI combination. The values in parentheses denote the best-fit parameters for this model.
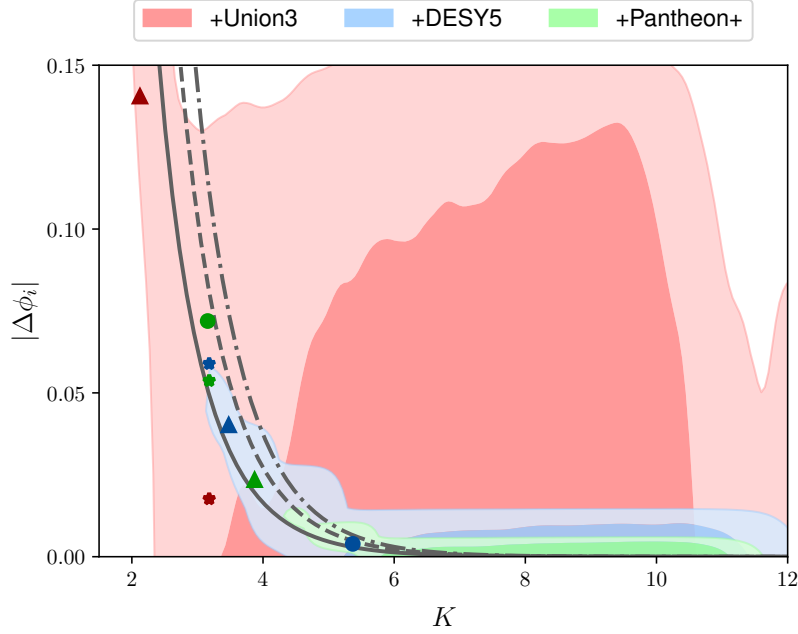

Figure 19. Analytical result from eq. (3.25), results for the hilltop quintessence models and posterior contours from MCMC analysis in the K-$|\Delta\phi_i|$ plane. The analytical result is in grey lines, where three different patterns use best-fit values for $\Omega_{\phi,0}$ and w_0 from different data combinations (solid: +Pantheon+, dashed: +Union3, dot-dashed: +DESY5). In the same figure, we show the 1σ and 2σ bounds from the constraints on the DS parameterisation for all data combinations. Values in the K-$|\Delta\phi_i|$ plane corresponding to the hilltop quintessence models are indicated by coloured shapes: circle for axion model, star for sugra model and triangle for the Higgs-like model, using best-fit values with Union3/Pantheon+/DESY5 for model parameters (ϕ_0 and f) denoted by dark blue/dark red/dark green shapes. All the best-fit values can be found in tables 6–9.

Figure 20. Derived bounds on $w_\phi(z = 0.4)$ from the MCMC analysis for the DS parameterisation.

## C Dutta-Scherrer-Chiba parameterisation, including curvature

In this appendix we collect the evolution of the equation of state including non-zero curvature, Ω_k and its comparison with the DS parameterisation, for all the models discussed in the main text. In all plots we take $\Omega_k = 0.005$.
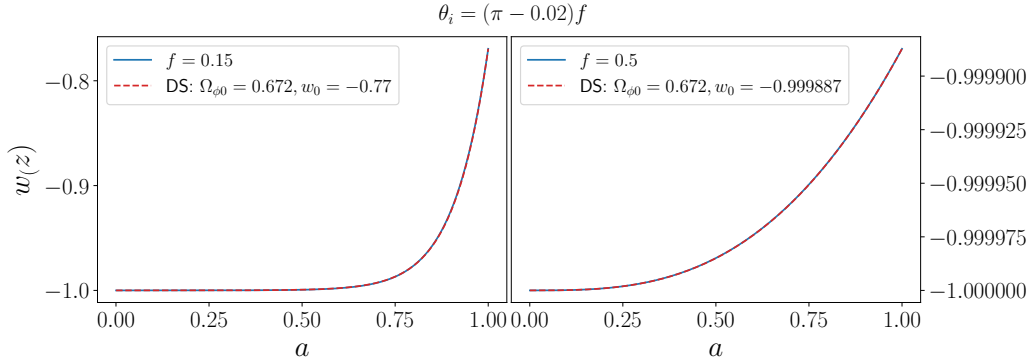
Figure 21. Evolution of $w_{\rm DE}$ for the Axion model including non-zero curvature and its comparison with the DS parameterisation.
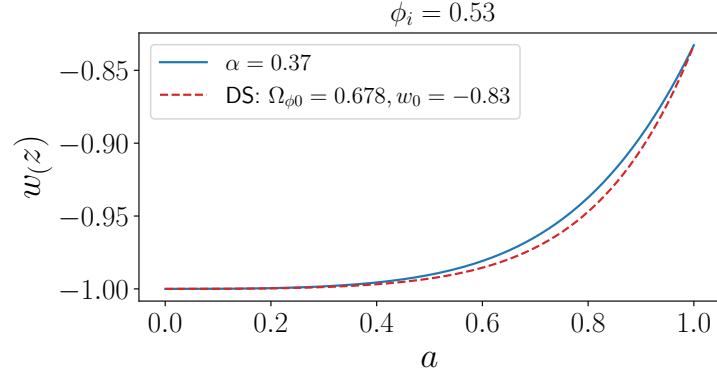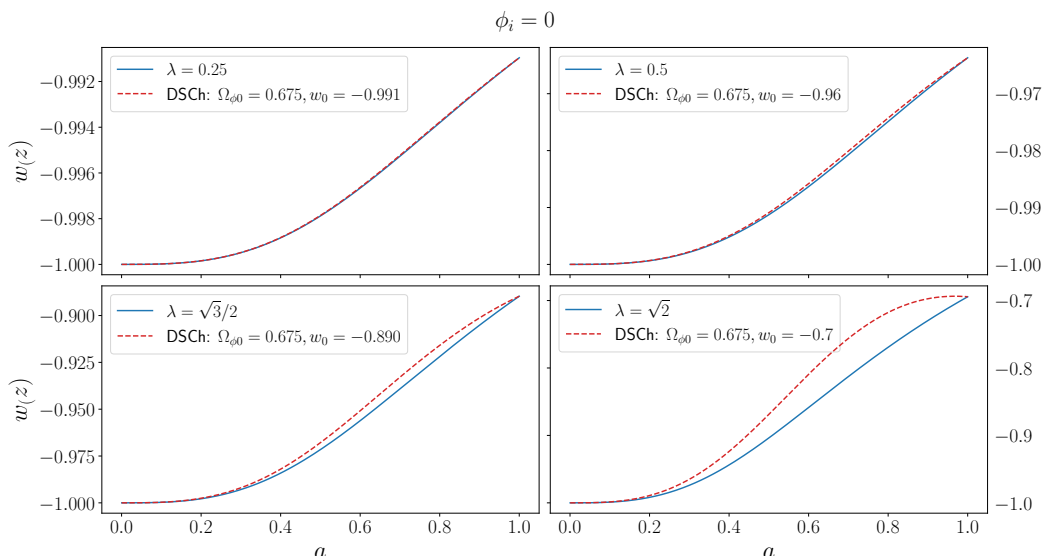
Figure 22. Evolution of w_{DE} for the Saxion model including non-zero curvature and its comparison with the DS parameterisation.
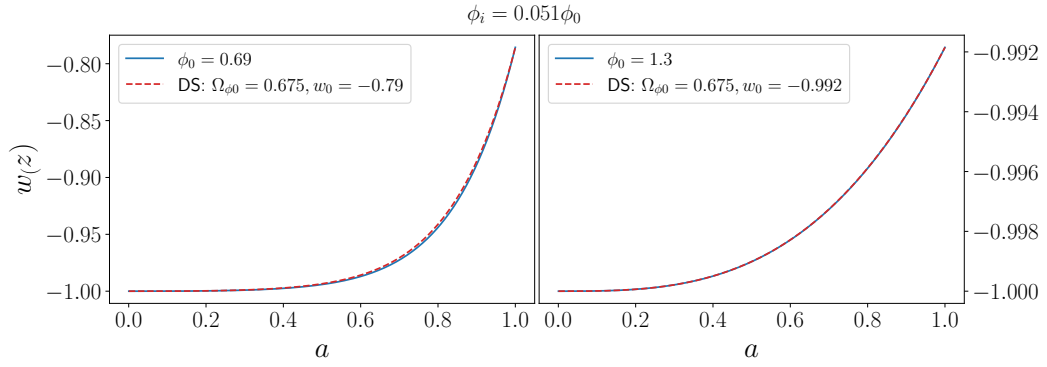
Figure 23. Evolution of w_{DE} for the Higgs-like model including non-zero curvature and its comparison with the DS parameterisation.

Figure 24. Evolution of w_{DE} for the Exponential model including non-zero curvature and its comparison with the DSCh parameterisation.

References

[1] M. Cicoli et al., *De Sitter vs quintessence in string theory*, *Fortsch. Phys.* **67** (2019) 1800079 [`arXiv:1808.08967`] [ɪɴSPIRE].

[2] M. Cicoli et al., *String cosmology: from the early universe to today*, *Phys. Rept.* **1059** (2024) 1 [`arXiv:2303.04819`] [ɪɴSPIRE].

[3] J. Polchinski, *The cosmological constant and the string landscape*, in the proceedings of the *23rd Solvay conference in physics: the quantum structure of space and time*, (2006) [`hep-th/0603249`] [ɪɴSPIRE].

[4] E. Palti, *The swampland: introduction and review*, *Fortsch. Phys.* **67** (2019) 1900037 [`arXiv:1903.06239`] [ɪɴSPIRE].

[5] M. van Beest, J. Calderón-Infante, D. Mirfendereski and I. Valenzuela, *Lectures on the swampland program in string compactifications*, *Phys. Rept.* **989** (2022) 1 [`arXiv:2102.01111`] [ɪɴSPIRE].

[6] M. Graña and A. Herráez, *The swampland conjectures: a bridge from quantum gravity to particle physics*, *Universe* **7** (2021) 273 [`arXiv:2107.00087`] [ɪɴSPIRE].

[7] S.K. Garg and C. Krishnan, *Bounds on slow roll and the de Sitter swampland*, *JHEP* **11** (2019) 075 [`arXiv:1807.05193`] [ɪɴSPIRE].

[8] H. Ooguri, E. Palti, G. Shiu and C. Vafa, *Distance and de Sitter conjectures on the swampland*, *Phys. Lett. B* **788** (2019) 180 [`arXiv:1810.05506`] [ɪɴSPIRE].

[9] E. Witten, *Quantum gravity in de Sitter space*, in the proceedings of the *Strings 2001: international conference*, (2001) [`hep-th/0106109`] [ɪɴSPIRE].

[10] T. Banks, *The top 10^{500} reasons not to believe in the landscape*, `arXiv:1208.5715` [ɪɴSPIRE].

[11] G. Dvali, C. Gomez and S. Zell, *Quantum breaking bound on de Sitter and swampland*, *Fortsch. Phys.* **67** (2019) 1800094 [`arXiv:1810.11002`] [ɪɴSPIRE].

[12] M. Cicoli et al., *Higher derivative corrections to string inflation*, *JHEP* **02** (2024) 115 [arXiv:2309.11697] [InSPIRE].

[13] T. Rudelius, *Dimensional reduction and (anti) de Sitter bounds*, *JHEP* **08** (2021) 041 [arXiv:2101.11617] [InSPIRE].

[14] B. Valeixo Bento, D. Chakraborty, S.L. Parameswaran and I. Zavala, *Dark energy in string theory*, *PoS* **CORFU2019** (2020) 123 [arXiv:2005.10168] [InSPIRE].

[15] D. Andriot et al., *Exponential quintessence: curved, steep and stringy?*, *JHEP* **08** (2024) 117 [arXiv:2405.09323] [InSPIRE].

[16] S. Bhattacharya et al., *Cosmological constraints on curved quintessence*, *JCAP* **09** (2024) 073 [arXiv:2405.17396] [InSPIRE].

[17] O.F. Ramadan, J. Sakstein and D. Rubin, *DESI constraints on exponential quintessence*, *Phys. Rev. D* **110** (2024) L041303 [arXiv:2405.18747] [InSPIRE].

[18] G. Alestas et al., *Is curvature-assisted quintessence observationally viable?*, *Phys. Rev. D* **110** (2024) 106010 [arXiv:2406.09212] [InSPIRE].

[19] S. Dutta and R.J. Scherrer, *Hilltop quintessence*, *Phys. Rev. D* **78** (2008) 123525 [arXiv:0809.4441] [InSPIRE].

[20] T. Chiba, *Slow-roll thawing quintessence*, *Phys. Rev. D* **79** (2009) 083517 [*Erratum ibid.* **80** (2009) 109902] [arXiv:0902.4037] [InSPIRE].

[21] M. Chevallier and D. Polarski, *Accelerating universes with scaling dark matter*, *Int. J. Mod. Phys. D* **10** (2001) 213 [gr-qc/0009008] [InSPIRE].

[22] E.V. Linder, *Exploring the expansion history of the universe*, *Phys. Rev. Lett.* **90** (2003) 091301 [astro-ph/0208512] [InSPIRE].

[23] R. Arjona and S. Nesseris, *A swampland conjecture DESIderátum?*, arXiv:2409.14990 [InSPIRE].

[24] S.L. Parameswaran, S. Ramos-Sanchez and I. Zavala, *On moduli stabilisation and de Sitter vacua in MSSM heterotic orbifolds*, *JHEP* **01** (2011) 071 [arXiv:1009.3931] [InSPIRE].

[25] D. Andriot, *Open problems on classical de Sitter solutions*, *Fortsch. Phys.* **67** (2019) 1900026 [arXiv:1902.10093] [InSPIRE].

[26] S. Parameswaran and M. Serra, *On (A)dS solutions from Scherk-Schwarz orbifolds*, *JHEP* **10** (2024) 039 [arXiv:2407.16781] [InSPIRE].

[27] W. Giarè, M.A. Sabogal, R.C. Nunes and E. Di Valentino, *Interacting dark energy after DESI baryon acoustic oscillation measurements*, *Phys. Rev. Lett.* **133** (2024) 251003 [arXiv:2404.15232] [InSPIRE].

[28] DES collaboration, *The Dark Energy Survey: cosmology results with ∼ 1500 new high-redshift type Ia supernovae using the full 5 yr data set*, *Astrophys. J. Lett.* **973** (2024) L14 [arXiv:2401.02929] [InSPIRE].

[29] DESI collaboration, *DESI 2024 VI: cosmological constraints from the measurements of baryon acoustic oscillations*, *JCAP* **02** (2025) 021 [arXiv:2404.03002] [InSPIRE].

[30] DESI collaboration, *DESI 2024: constraints on physics-focused aspects of dark energy using DESI DR1 BAO data*, *Phys. Rev. D* **111** (2025) 023532 [arXiv:2405.13588] [InSPIRE].

[31] J.A. Frieman, C.T. Hill, A. Stebbins and I. Waga, *Cosmology with ultralight pseudo Nambu-Goldstone bosons*, *Phys. Rev. Lett.* **75** (1995) 2077 [astro-ph/9505060] [InSPIRE].

[32] K. Choi, *String or M theory axion as a quintessence*, *Phys. Rev. D* **62** (2000) 043509 [hep-ph/9902292] [InSPIRE].

[33] J.E. Kim and H.P. Nilles, *A quintessential axion*, *Phys. Lett. B* **553** (2003) 1 [hep-ph/0210402] [InSPIRE].

[34] P. Svrcek, *Cosmological constant and axions in string theory*, hep-th/0607086 [InSPIRE].

[35] N. Kaloper and L. Sorbo, *Where in the string landscape is quintessence*, *Phys. Rev. D* **79** (2009) 043528 [arXiv:0810.5346] [InSPIRE].

[36] S. Panda, Y. Sumitomo and S.P. Trivedi, *Axions as quintessence in string theory*, *Phys. Rev. D* **83** (2011) 083506 [arXiv:1011.5877] [InSPIRE].

[37] A. Arvanitaki et al., *String axiverse*, *Phys. Rev. D* **81** (2010) 123530 [arXiv:0905.4720] [InSPIRE].

[38] N. Arkani-Hamed, L. Motl, A. Nicolis and C. Vafa, *The string landscape, black holes and gravity as the weakest force*, *JHEP* **06** (2007) 060 [hep-th/0601001] [InSPIRE].

[39] J.E. Kim, H.P. Nilles and M. Peloso, *Completing natural inflation*, *JCAP* **01** (2005) 005 [hep-ph/0409138] [InSPIRE].

[40] S. Dimopoulos, S. Kachru, J. McGreevy and J.G. Wacker, *N-flation*, *JCAP* **08** (2008) 003 [hep-th/0507205] [InSPIRE].

[41] R.T. Co, E. Gonzalez and K. Harigaya, *Axion misalignment driven to the hilltop*, *JHEP* **05** (2019) 163 [arXiv:1812.11192] [InSPIRE].

[42] J.P. Conlon, *The de Sitter swampland conjecture and supersymmetric AdS vacua*, *Int. J. Mod. Phys. A* **33** (2018) 1850178 [arXiv:1808.05040] [InSPIRE].

[43] L. McAllister, J. Moritz, R. Nally and A. Schachner, *Candidate de Sitter vacua*, *Phys. Rev. D* **111** (2025) 086015 [arXiv:2406.13751] [InSPIRE].

[44] Y. Olguin-Trejo, S.L. Parameswaran, G. Tasinato and I. Zavala, *Runaway quintessence, out of the swampland*, *JCAP* **01** (2019) 031 [arXiv:1810.08634] [InSPIRE].

[45] J. Louis, M. Rummel, R. Valandro and A. Westphal, *Building an explicit de Sitter*, *JHEP* **10** (2012) 163 [arXiv:1208.3208] [InSPIRE].

[46] F. Carta, J. Moritz and A. Westphal, *Gaugino condensation and small uplifts in KKLT*, *JHEP* **08** (2019) 141 [arXiv:1902.01412] [InSPIRE].

[47] E. Hardy and S. Parameswaran, *Thermal dark energy*, *Phys. Rev. D* **101** (2020) 023503 [arXiv:1907.10141] [InSPIRE].

[48] J.M. Gomes, E. Hardy and S. Parameswaran, *Dark energy with the help of interacting dark sectors*, *Phys. Rev. D* **110** (2024) 023533 [arXiv:2311.08888] [InSPIRE].

[49] P. Sikivie, *Axion cosmology*, *Lect. Notes Phys.* **741** (2008) 19 [astro-ph/0610440] [InSPIRE].

[50] H. Ooguri and C. Vafa, *On the geometry of the string landscape and the swampland*, *Nucl. Phys. B* **766** (2007) 21 [hep-th/0605264] [InSPIRE].

[51] G. Pantazis, S. Nesseris and L. Perivolaropoulos, *Comparison of thawing and freezing dark energy parametrizations*, *Phys. Rev. D* **93** (2016) 103503 [arXiv:1603.02164] [InSPIRE].

[52] I.D. Gialamas et al., *Interpreting DESI 2024 BAO: late-time dynamical dark energy or a local effect?*, *Phys. Rev. D* **111** (2025) 043540 [arXiv:2406.07533] [InSPIRE].

[53] Y. Akrami, R. Kallosh, A. Linde and V. Vardanyan, *The landscape, the swampland and the era of precision cosmology*, *Fortsch. Phys.* **67** (2019) 1800075 [`arXiv:1808.09440`] [ɪɴSPIRE].

[54] PLANCK collaboration, *Planck 2018 results. V. CMB power spectra and likelihoods*, *Astron. Astrophys.* **641** (2020) A5 [`arXiv:1907.12875`] [ɪɴSPIRE].

[55] E. Rosenberg, S. Gratton and G. Efstathiou, *CMB power spectra and cosmological parameters from Planck PR4 with CamSpec*, *Mon. Not. Roy. Astron. Soc.* **517** (2022) 4620 [`arXiv:2205.10869`] [ɪɴSPIRE].

[56] PLANCK collaboration, *Planck 2018 results. VIII. Gravitational lensing*, *Astron. Astrophys.* **641** (2020) A8 [`arXiv:1807.06210`] [ɪɴSPIRE].

[57] DESI collaboration, *DESI 2024 IV: baryon acoustic oscillations from the Lyman α forest*, *JCAP* **01** (2025) 124 [`arXiv:2404.03001`] [ɪɴSPIRE].

[58] DESI collaboration, *DESI 2024 III: baryon acoustic oscillations from galaxies and quasars*, *JCAP* **04** (2025) 012 [`arXiv:2404.03000`] [ɪɴSPIRE].

[59] D. Brout et al., *The Pantheon+ analysis: cosmological constraints*, *Astrophys. J.* **938** (2022) 110 [`arXiv:2202.04077`] [ɪɴSPIRE].

[60] D. Rubin et al., *Union through UNITY: cosmology with 2,000 SNe using a unified Bayesian framework*, [`arXiv:2311.12098`] [ɪɴSPIRE].

[61] A. Lewis and S. Bridle, *Cosmological parameters from CMB and other data: a Monte Carlo approach*, *Phys. Rev. D* **66** (2002) 103511 [`astro-ph/0205436`] [ɪɴSPIRE].

[62] A. Lewis, *Efficient sampling of fast and slow cosmological parameters*, *Phys. Rev. D* **87** (2013) 103529 [`arXiv:1304.4473`] [ɪɴSPIRE].

[63] J. Torrado and A. Lewis, *Cobaya: code for Bayesian analysis of hierarchical physical models*, *JCAP* **05** (2021) 057 [`arXiv:2005.05290`] [ɪɴSPIRE].

[64] A. Lewis, *GetDist: a python package for analysing Monte Carlo samples*, [`arXiv:1910.13970`] [ɪɴSPIRE].

[65] C. Cartis, L. Roberts and O. Sheridan-Methven, *Escaping local minima with local derivative-free methods: a numerical investigation*, *Optimization* **71** (2021) 2343 [`arXiv:1812.11343`] [ɪɴSPIRE].

[66] C. Cartis, J. Fiala, B. Marteau and L. Roberts, *Improving the flexibility and robustness of model-based derivative-free optimization solvers*, [`arXiv:1804.00154`] [ɪɴSPIRE].

[67] DESI collaboration, *DESI 2024: reconstructing dark energy using crossing statistics with DESI DR1 BAO data*, *JCAP* **10** (2024) 048 [`arXiv:2405.04216`] [ɪɴSPIRE].

[68] DESI collaboration, *DESI 2024: constraints on physics-focused aspects of dark energy using DESI DR1 BAO data*, *Phys. Rev. D* **111** (2025) 023532 [`arXiv:2405.13588`] [ɪɴSPIRE].

[69] S. Roy Choudhury and T. Okumura, *Updated cosmological constraints in extended parameter space with Planck PR4, DESI baryon acoustic oscillations, and supernovae: dynamical dark energy, neutrino masses, lensing anomaly, and the Hubble tension*, *Astrophys. J. Lett.* **976** (2024) L11 [`arXiv:2409.13022`] [ɪɴSPIRE].

[70] E.Ó. Colgáin et al., *Does DESI 2024 confirm ΛCDM?*, [`arXiv:2404.08633`] [ɪɴSPIRE].

[71] Y. Carloni, O. Luongo and M. Muccino, *Does dark energy really revive using DESI 2024 data?*, *Phys. Rev. D* **111** (2025) 023512 [`arXiv:2404.12068`] [ɪɴSPIRE].

[72] C.-G. Park, J. de Cruz Pérez and B. Ratra, *Using non-DESI data to confirm and strengthen the DESI 2024 spatially flat $w_0 w_a CDM$ cosmological parametrization result*, *Phys. Rev. D* **110** (2024) 123533 [arXiv:2405.00502] [ɪɴSPIRE].

[73] D. Wang, *The self-consistency of DESI analysis and comment on "Does DESI 2024 confirm ΛCDM?"*, arXiv:2404.13833 [ɪɴSPIRE].

[74] M. Cortês and A.R. Liddle, *Interpreting DESI's evidence for evolving dark energy*, *JCAP* **12** (2024) 007 [arXiv:2404.08056] [ɪɴSPIRE].

[75] Z. Wang, S. Lin, Z. Ding and B. Hu, *The role of LRG1 and LRG2's monopole in inferring the DESI 2024 BAO cosmology*, *Mon. Not. Roy. Astron. Soc.* **534** (2024) 3869 [arXiv:2405.02168] [ɪɴSPIRE].

[76] B.R. Dinda, *A new diagnostic for the null test of dynamical dark energy in light of DESI 2024 and other BAO data*, *JCAP* **09** (2024) 062 [arXiv:2405.06618] [ɪɴSPIRE].

[77] K.S. Croker et al., *DESI dark energy time evolution is recovered by cosmologically coupled black holes*, *JCAP* **10** (2024) 094 [arXiv:2405.12282] [ɪɴSPIRE].

[78] D. Wang, *Constraining cosmological physics with DESI BAO observations*, arXiv:2404.06796 [ɪɴSPIRE].

[79] O. Luongo and M. Muccino, *Model-independent cosmographic constraints from DESI 2024*, *Astron. Astrophys.* **690** (2024) A40 [arXiv:2404.07070] [ɪɴSPIRE].

[80] P. Mukherjee and A.A. Sen, *Model-independent cosmological inference post DESI DR1 BAO measurements*, *Phys. Rev. D* **110** (2024) 123502 [arXiv:2405.19178] [ɪɴSPIRE].

[81] H. Wang and Y.-S. Piao, *Dark energy in light of recent DESI BAO and Hubble tension*, arXiv:2404.18579 [ɪɴSPIRE].

[82] G. Efstathiou, *Evolving dark energy or supernovae systematics?*, *Mon. Not. Roy. Astron. Soc.* **538** (2025) 875 [arXiv:2408.07175] [ɪɴSPIRE].

[83] Y. Tada and T. Terada, *Quintessential interpretation of the evolving dark energy in light of DESI observations*, *Phys. Rev. D* **109** (2024) L121305 [arXiv:2404.05722] [ɪɴSPIRE].

[84] W. Yin, *Cosmic clues: DESI, dark energy, and the cosmological constant problem*, *JHEP* **05** (2024) 327 [arXiv:2404.06444] [ɪɴSPIRE].

[85] K.V. Berghaus, J.A. Kable and V. Miranda, *Quantifying scalar field dynamics with DESI 2024 Y1 BAO measurements*, *Phys. Rev. D* **110** (2024) 103524 [arXiv:2404.14341] [ɪɴSPIRE].

[86] D. Shlivko and P.J. Steinhardt, *Assessing observational constraints on dark energy*, *Phys. Lett. B* **855** (2024) 138826 [arXiv:2405.03933] [ɪɴSPIRE].

[87] G. Alestas, M. Caldarola, S. Kuroyanagi and S. Nesseris, *DESI constraints on α-attractor inflationary models*, *Phys. Rev. D* **111** (2025) 083506 [arXiv:2410.00827] [ɪɴSPIRE].

[88] S. Sohail, S. Alam, S. Akthar and M.W. Hossain, *Quintessential early dark energy*, arXiv:2408.03229 [ɪɴSPIRE].

[89] D. Andriot, *Quintessence: an analytical study, with theoretical and observational applications*, arXiv:2410.17182 [ɪɴSPIRE].

[90] W. Giarè, *Dynamical dark energy beyond Planck? Constraints from multiple CMB probes, DESI BAO and type-Ia supernovae*, arXiv:2409.17074 [ɪɴSPIRE].

[91] W. Giarè et al., *Robust preference for dynamical dark energy in DESI BAO and SN measurements*, *JCAP* **10** (2024) 035 [arXiv:2407.16689] [ɪɴSPIRE].

[92] W.J. Wolf and P.G. Ferreira, *Underdetermination of dark energy*, *Phys. Rev. D* **108** (2023) 103519 [arXiv:2310.07482] [InSPIRE].

[93] M. Cicoli, F. Cunillera, A. Padilla and F.G. Pedro, *From inflation to quintessence: a history of the universe in string theory*, *JHEP* **10** (2024) 141 [arXiv:2407.03405] [InSPIRE].

[94] M. Cicoli, F.G. Pedro and G. Tasinato, *Natural quintessence in string theory*, *JCAP* **07** (2012) 044 [arXiv:1203.6655] [InSPIRE].

[95] N. Schöneberg et al., *News from the swampland — constraining string theory with astrophysics and cosmology*, *JCAP* **10** (2023) 039 [arXiv:2307.15060] [InSPIRE].

[96] W.J. Wolf, C. García-García, D.J. Bartlett and P.G. Ferreira, *Scant evidence for thawing quintessence*, *Phys. Rev. D* **110** (2024) 083528 [arXiv:2408.17318] [InSPIRE].

[97] H. Akaike, *A new look at the statistical model identification*, *IEEE Trans. Automatic Control* **19** (1974) 716 [InSPIRE].

[98] A.R. Liddle, *How many cosmological parameters?*, *Mon. Not. Roy. Astron. Soc.* **351** (2004) L49 [astro-ph/0401198] [InSPIRE].

[99] R.J. Scherrer, *Mapping the Chevallier-Polarski-Linder parametrization onto physical dark energy models*, *Phys. Rev. D* **92** (2015) 043001 [arXiv:1505.05781] [InSPIRE].

[100] B. Heidenreich, M. Reece and T. Rudelius, *Sharpening the weak gravity conjecture with dimensional reduction*, *JHEP* **02** (2016) 140 [arXiv:1509.06374] [InSPIRE].